Environ Monit Assess (2025) 197:242
https://doi.org/10.1007/s10661-025-13686-3

RESEARCH

A Novel Agricultural Remote Sensing Drought Index (ARSDI) for high-resolution drought assessment in Africa using Sentinel and Landsat data

Nasser A. M. Abdelrahim · Shuanggen Jin

Received: 20 November 2024 / Accepted: 24 January 2025

Abstract Drought poses a significant threat to agricultural productivity in Africa due to climate variability and water scarcity. To improve drought monitoring using high-resolution remote sensing data, this paper proposes a novel Agricultural Remote Sensing Drought Index (ARSDI). Imagery from Sentinel-1(S-1), Sentinel-2 (S-2), and Landsat 8 was utilized to develop a drought monitoring system for 2017–2023, during which Egypt and Kenya experienced significant drought events. In Kenya, particularly from 2021 to 2023, recurrent droughts severely affected agricultural output, necessitating the evaluation of ARSDI's efficiency in capturing drought severity. Similarly, in Egypt, drought-like conditions linked to reduced Nile River flow and rainfall variability posed significant challenges. ARSDI exhibited strong correlations with traditional drought indicators, such as the Soil Moisture Condition Index (SMCI), ranging from 0.64 to 0.88 in Egypt and 0.74 to 0.85 in Kenya. It also correlated well with the Vegetation Health Index (VHI), with values (0.96 to 0.98) in Egypt and (0.53 to 0.98) in Kenya. Furthermore, ARSDI aligned with Standardized Precipitation Index (SPI), ranging (0.44 to 0.71) in Egypt and (0.47 to 0.60) in Kenya. By integrating Sentinel-1 radar data, ARSDI mitigated the limitations of cloud cover, providing more reliable vegetation monitoring. Compared to other indices, such as the Normalized Difference Vegetation Index (NDVI), ARSDI exhibited superior performance, particularly during the drought events 2019 in Egypt and 2020 in Kenya, demonstrating its robustness in assessing soil moisture and vegetation health.

Keywords Agricultural drought · Drought index · Soil moisture · NDVI

N. A. M. Abdelrahim (✉) · S. Jin
Shanghai Astronomical Observatory, Chinese Academy of Sciences, Shanghai 200030, China
e-mail: nasserahmed@shao.ac.cn; nasserahmed3311@gmail.com

S. Jin
e-mail: sgjin@shao.ac.cn; sg.jin@yahoo.com

N. A. M. Abdelrahim
School of Astronomy and Space Science, University of Chinese Academy of Sciences, Beijing 100049, China

N. A. M. Abdelrahim
Civil Engineering Department, Faculty of Engineering, Sohag University, Sohag 82511, Egypt

S. Jin
School of Surveying and Land Information Engineering, Henan Polytechnic University, Jiaozuo 454003, China

Introduction

One of the greatest serious natural disasters that affects agriculture, environmental variables, and socioeconomic circumstances is drought (Edokossi et al., 2024; Elameen et al., 2023; Jin & Zhang, 2016; Shorachi et al., 2022). According to Li et al. (2024), a drought is a phenomenon that is defined

by a shortage of water caused by anomalous behavior components in the hydro-climatic system, such as rising temperatures, dropping precipitation, and relative humidity. Food production levels, livelihoods, and natural ecosystems in the broader Horn of Africa have all been negatively impacted by drought (Alito & Kerebih, 2024). According to Shen et al. (2019), drought can take four distinct forms: hydrological, agricultural, economic, and meteorological. A very low precipitation spell lasting several months or even years is known as a meteorological drought. Groundwater, streamflow, or total water storage that is lower than long-term averages results in a hydrological drought. Dry conditions that result in higher demand than supply for specific goods are referred to as socioeconomic droughts (Khorrami & Gündüz, 2022). The most difficult and poorly understood of these is the agricultural drought. Alkaraki and Hazaymeh (2023) state that when soil moisture content declines and crops cannot be supplied with enough water throughout the growing season, an agricultural drought occurs. This is attributable to several variables, including anomalous rainfall, rising temperatures, and disruptions in normal rainfall patterns.

In order to manage water resources, mitigate droughts, and even ensure national food security, it is imperative that agricultural droughts be promptly and efficiently monitored (Wu et al., 2021). For over 50 years, researchers have developed various techniques and metrics to monitor and analyze droughts. These methodologies utilize catalyst parameters, such as evapotranspiration, soil moisture, temperature, precipitation, and humidity, as well as response parameters, such as groundwater levels, vegetation health, and reservoir and plant health (Afzal & Ragab, 2019). Data for tracking agricultural drought is gathered by on-site or remote sensing methods (such as satellites), and this data can be used to research or create drought indicators (Liu et al., 2020). In light of Hayes et al. (n.d.), a drought index is a numerical representation that may be used to determine the duration and severity of a drought by combining one or more physical indices. Based on the type of drought, drought indices were categorized and then separated into conventional/region-specific and remote sensing categories based on the type of data used. Additionally, the drought indices based on remote sensing data, divided into simple indices including microwave, thermal, and optical as well as composite indices (Alahacoon & Edirisinghe, 2022; Holben, 1980; Felix N. Kogan, 1995a, 1995b). Palmer Drought Severity Index (PDSI) (Li & Cai, 2024; Palmer and Wayne, 1965), Standardized Precipitation Index (SPI) (Sakellariou et al., 2024), and Standardized Precipitation Evapotranspiration Index (SPEI) (Dong et al., 2023; Vicente-Serrano et al., 2010) are the most commonly used drought indices derived from site data. These indices, which primarily offer precise assessments of agricultural drought conditions in specific places, depend on agroclimatic stations' in situ readings of soil moisture, evapotranspiration, and precipitation. Nevertheless, because of their sparse distribution and small numbers, these agroclimatic stations lack the geographical representative aspect of agricultural drought (Hazaymeh & Hassan, 2017).

Assessment of the drought has benefited greatly over the past few years by the use of high-resolution model data and remote sensing (Edokossi et al., 2020; Jin et al., 2022, 2024; Najibi & Jin, 2013). Real-time data from the atmosphere, soil, and plants can be obtained using remote sensing (Kulkarni et al., 2020). The unique spectral properties of the canopy and soil surface, particularly in the thermal, shortwave infrared, near-infrared, and red spectral bands, serve as the foundation for remote sensing indices. The basic concept behind using remote sensing for detecting drought in agricultural lands is that the properties of soil and vegetation, including soil temperature, organic matter, chlorophyll, biomass, and canopy, may be affected by drought. According to Dalezios et al. (2012), this could alter their thermal and spectral responses, which can be employed as markers of the onset of drought. Currently, most studies were concentrated on the creation of concepts for drought monitoring and indices using data from remote sensing for various applications (Afshar et al., 2021; Araneda-Cabrera et al., 2021; Corbari et al., 2024; Dos Santos Araujo et al., 2024; Khorrami et al., 2023; Khorrami & Gunduz, 2021; Li et al., 2024; Qin et al., 2021; Sánchez et al., 2016; Schwabe et al., 2013; Shahzaman et al., 2021; Skakun et al., 2016; Tang & Li, 2014; Tian et al., 2018; X. Zhang et al., 2017a, 2017b), such as the normalized difference vegetation index (NDVI) (Thenkabail et al., 1994), Shortwave Infrared Water Stress Index (SIWSI) (Fensholt & Sandholt, 2003), Visible and Shortwave Drought Index (VSDI) (Zhang et al., 2013), Vegetation Condition Index (VCI) (F.N. Kogan, 1995a, 1995b), Soil

Adjusted Vegetation Index (SAVI) (Huete, 1988), Temperature Condition Index (TCI) (Kogan, 1997), Normalized Difference Infrared Indexes (NDII) (Fensholt & Sandholt, 2003), Vegetation Health Index (VHI) (Alahacoon et al., 2021; Bhuiyan et al., 2006), and Soil Moisture Condition Index (SMCI) (Zhang & Jia, 2013).

High-resolution data on the state of agricultural drought that is continuously captured, both geographically and temporally, is needed to address this increased risk of drought (Dotzler et al., 2015). More and more, near-real-time, multi-temporal, and regional Earth observation (EO) applications using Sentinel-2 (S-2) sceneries are being used (Sudmanns et al., 2020). The restricted availability of optical data resulting from cloud cover is a significant drawback. However, because of their ability to gather data concerning any weather circumstances and at night, Synthetic Aperture Radar (SAR) systems like Sentinel-1 (S-1) may be able to significantly close these monitoring gaps (Felegari et al., 2021; Kaiser et al., 2022). Understanding the earth's surface's thermal behavior and drought monitoring depend heavily on LST estimation (Pande et al., 2024). Using Google Earth Engine GEE (Mullissa et al., 2021; Teluguntla et al., 2018), a cloud-based platform that makes remote sensing data analysis and processing easier, is one of the efficient ways to estimate LST. Thermal infrared data from sensors such as Landsat-8 is among the several satellite imagery options provided by GEE (Pande et al., 2023; Ren et al., 2021). With time series showing processes on the Earth's surface, the increased availability of data opens up new possibilities for temporal as well as spatial data analysis (Urban et al., 2018).

The majority of current drought indices rely on coarse resolution data with a range of 250 m to 1 km, despite notable improvements in drought monitoring. The localized subtleties of drought conditions are frequently missed by these intermediate to coarse resolution datasets, such as those from MODIS, especially in varied environments. Additionally, very little research has been done on drought monitoring in Africa, a continent that is extremely susceptible to both water scarcity and climate variability (Atzberger, 2013; Brandt et al., 2016; Malakar & Hulley, 2016; Tran et al., 2017; Trnka et al., 2020; Winkler et al., 2017). However, the fact that these integrated, remotely sensed indices were created and assessed for a particular climatic or geographic area severely limits their applicability (X. Zhang et al., 2017a, 2017b). Generally, the indices were established across study areas that are limited to a single climate region. A few of these indices were created in a variety of settings spanning wide geographic areas. If specific indices are utilized in climate zones that differ significantly from those in which they were established, this geographic restriction may result in subpar performance (Quiring & Ganesh, 2010).

This research aims to address these gaps by developing a high-resolution Agricultural Remote Sensing Drought Index (ARSDI) using S-1, S-2, and Landsat data by integrating multiple indices through Principal Component Analysis (PCA) (Arun Kumar et al., 2021; Du et al., 2013; Son et al., 2021). This approach not only enhances spatial resolution but also offers timely and accurate drought information, which is essential to efficient resource management and policymaking in drought-prone regions of Africa. The focus on two study areas (Egypt and Kenya) demonstrates the versatility and applicability of ARSDI across diverse environments (Jiao et al., 2019; Zhang & Zhou, 2015), further underscoring the need for high-resolution, region-specific drought monitoring tools in addressing the pressing challenges of climate change and water scarcity in Africa. The rest of this paper is consistent with materials and methods in the "Methods" section; the "Results and discussions" section contains results, analysis, and discussions; and the conclusion is given in the "Conclusion" section.

Materials

Study areas

The study areas are located in Egypt and Kenya, inside highly agriculturally practiced regions. In Egypt, the area of interest is around a center point of 31.051°N, 30.769°E. The area largely includes parts of the Nile Delta and Nile Valley, surrounded by richly grown fields of agriculture. The area is arid with just 24 mm of rainfall each year; the bulk of it is during winter. By far, the most crucial activity in the area is in irrigated agriculture from the Nile River. The most common crops in this region include wheat, maize, rice, and cotton. Surrounding the

well-manured land is buildings with bare soil (Fawzy et al., 2021; Khater et al., 2015).

The study region in Kenya stands at a center point of − 0.645°S, 36.379°E, and generally, it falls within the central highlands and part of the Rift Valley, with a wide range from semi-arid to more humid conditions. In this area, the yearly average of precipitation ranges between 500 and 1500 mm. The agricultural lands here are critical to Kenya's food security. Major crops include maize, beans, coffee, and tea. It also includes the regions that are dry or semi-dry in the surrounding areas that suffer frequent droughts affecting subsistence farming and pastoralism (Masinde, 2015; Opiyo et al., 2014). Both Egypt and Kenya were chosen as study areas for their striking variation in climatic conditions from arid irrigation-dependent agriculture to semi-arid and humid zones, thus providing a varied test bed for the adaptability and performance of ARSDI. Figure 1 shows the land cover type of these study areas using GEE.

Data acquisition

In this study, drought conditions in Africa from 2017 to 2023 have been evaluated using satellite data from Sentinel-1, Sentinel-2, and Landsat 8. Using Google Earth Engine, a potent tool for planetary-scale environmental data research, the data was retrieved and preprocessed.

Data from the EU's Copernicus program using Sentinel-1 synthetic aperture radar is exceptional since it provides high temporal density and high-resolution SAR satellite images for the entire world for the first time. With the help of the cloud-penetrating radar, observations can be taken virtually continuously during the day and night and in almost any

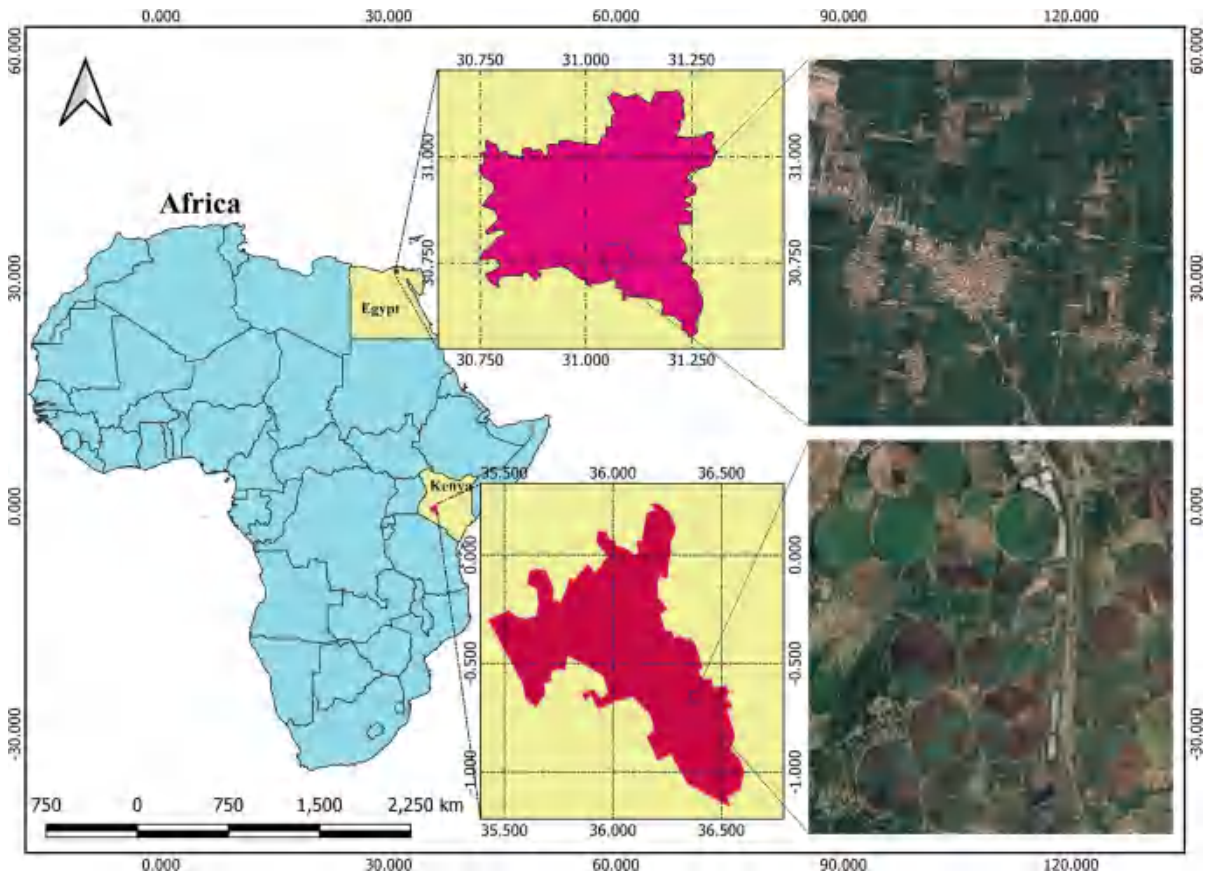

Fig. 1 Land cover types of study areas in Egypt and Kenya using Google Earth Engine. This map shows the distribution of agricultural fields, urban areas, and other land covers within the arid Nile Delta region of Egypt and the diverse climatic zones of the central highlands of Kenya

kind of weather (Mullissa et al., 2021). Numerous research (Mohseni et al., 2023; Mullissa et al., 2021; Nasirzadehdizaji et al., 2021; Shorachi et al., 2022; Vreugdenhil et al., 2018) have demonstrated the usefulness of S-1 SAR images for agricultural growth monitoring. S-1 has a unique opportunity to record crops' drought response because of backscatter's sensitivity to vegetation water content and geometry (Kaiser et al., 2022).

With a better temporal resolution of 5 days, the S-2Multispectral Instrument (MSI) comprises two spacecraft for Earth observation at spatial resolutions of 10 m, 20 m, and 60 m (Kumari & Karthikeyan, 2023; Phiri et al., 2020). Among the publicly accessible satellite products, the maximum spatial resolution is 10 m. Three bands of red edge that are capable of capturing the rich near-infrared reflectance of plants is another distinctive feature of the S-2 data (Abdi, 2020; Liu et al., 2020).

The most crucial factor in predicting and calculating soil moisture, plant drought stress, and evapotranspiration is the land surface temperature (LST). LST was estimated using temperature and emissivity separation (TES) algorithm (Khorrami & Gunduz, 2020; Tao et al., 2024). The Landsat 8 satellite is fitted with an Operational Land Imager (OLI) and a Thermal Infrared Sensor (TIRS). According to Mancino et al. (2020) and Maulana and Bioresita (2023), Landsat 8 includes two thermal bands (for 10 and 11) (resampled to 30 m) with a spatial resolution of 100 m, nine spectral bands (for bands 1 to 7) with a spatial resolution of 30 m, and eight panchromatic bands with a resolution of 15 m. This study's remote sensing data features are compiled in Table 1.

Methodology

This research employs a comprehensive methodology to develop and validate the Agricultural Remote Sensing Drought Index (ARSDI) using data from S-1, S-2, and Landsat 8. The combination of the soil, vegetation, and atmosphere leads to agricultural drought. Therefore, when creating the ARSDI, this study considered a number of drought-causing elements. The whole procedure is constituted by several steps: data preparation and preprocessing in Google Earth Engine; compute the Novel Hybrid Vegetation Index by using S-1 and S-2 data to improve the performance of NDVI; compute in the third stage the following vegetation indices: Green Normalized Difference Vegetation Index (GNDVI), Soil Adjusted Vegetation Index (SAVI), Temperature Condition Index (TCI), Normalized Difference Infrared Index (NDII), and Vegetation Condition Index (VCI). In the fourth step, these indices are integrated using Principal Component Analysis (PCA). The first PCA-derived component is used to form the Agricultural Remote Sensing Drought Index (ARSDI). The fifth step was the validation of ARSDI against established drought indices such as the Vegetation Health Index (VHI), the Soil Moisture Condition Index (SMCI), and Standard Precipitation Index (SPI). Finally, the performance of the ARSDI was compared with several other drought indices (Normalized Difference Vegetation Index (NDVI), Surface Water Capacity Index (SWCI), Shortwave infrared Soil Moisture Index (SIMI), and Visible and Shortwave Drought Index (VSDI). Figure 2 illustrates the methodology steps.

Table 1 Characteristics of remote sensing datasets used in ARSDI development. This includes satellite instrument, spectral bands, spatial and temporal resolutions, and GEE collection

Satellite	Instrument	Bands	Spatial resolution	Temporal resolution	GEE collection
Sentinel-1	SAR (C-band)	VV, VH	10 m	6–12 days	COPERNICUS/S1_GRD
Sentinel-2	MSI	B2 (Blue), B3 (Green), B4 (Red), B8 (NIR), B11 (SWIR1), B12 (SWIR2)	10 m (B2, B3, B4, B8), 20 m (B11, B12)	5 days	COPERNICUS/S2
Landsat 8	OLI and TIRS	B 2 (Blue), B 3 (Green), B 4 (Red), B 5 (NIR), B 6 (SWIR1), B 7 (SWIR2), B 10 (TIRS1), B 11 (TIRS2)	30 m (OLI bands), 100 m (TIRS bands resampled to 30 m)	16 days	LANDSAT/LC08/C01/T1_SR

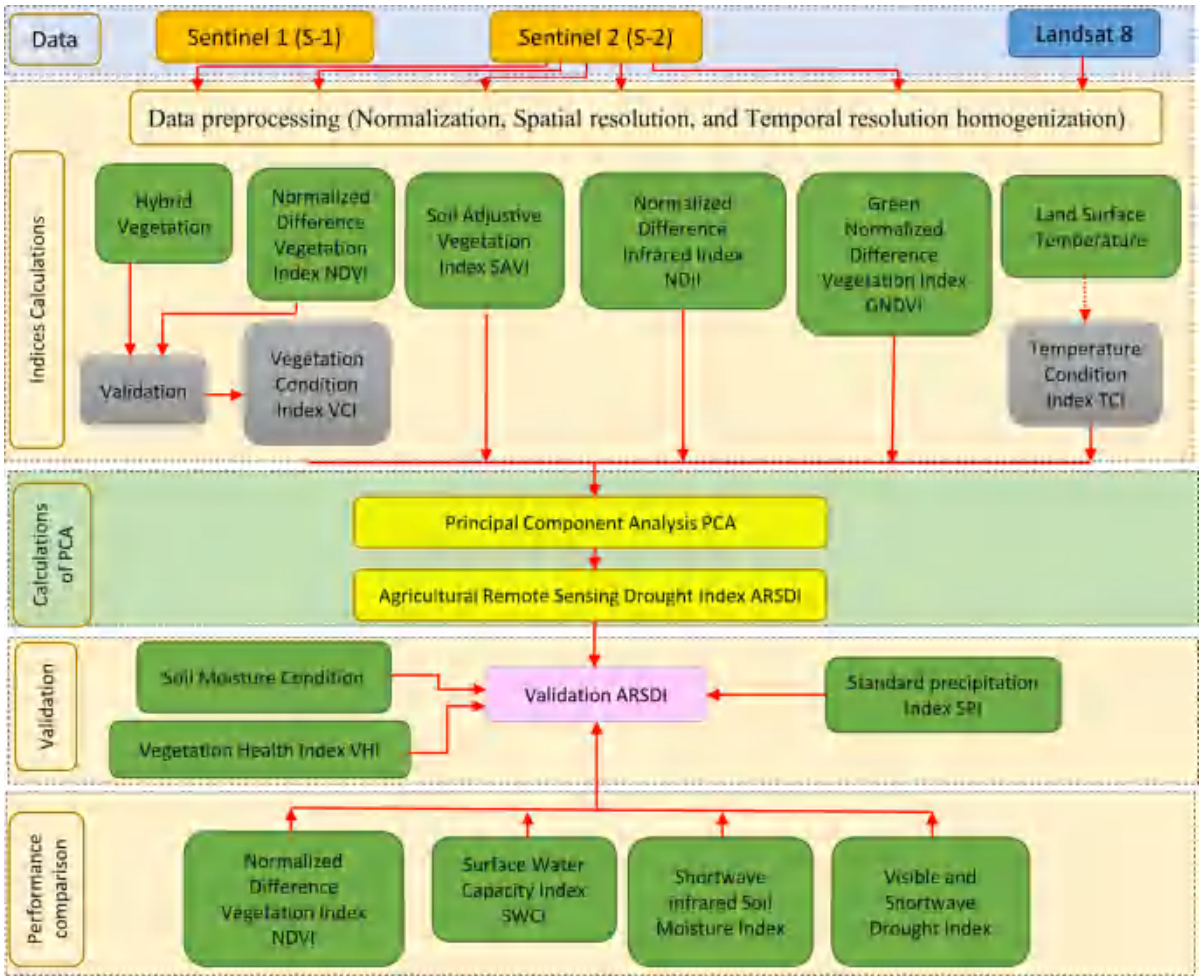

Fig. 2 Workflow of the methodology for developing the Agricultural Remote Sensing Drought Index (ARSDI). The process includes data preprocessing, computation of vegetation indices, Principal Component Analysis (PCA) integration, and validation against established drought indices

Data preprocessing

Prior to integrating S-1, S-2, and Landsat-8, for the calculation of the HVI and the other drought-related indices, data compatibility was considered by applying certain normalizing steps (Bhogapurapu et al., 2022; Kaushik & Jabin, 2018; Mullissa et al., 2021). The normalization of S-1 radar backscatter coefficients was performed by transforming the original VV and VH in decibels (dB) into a linear scale, using Eq. (1). This scaling brought the radar data into the scale of reflectance values from optical sensors (Braun & Veci, 2015; Small, 2011). Later, all data, including radar and optical, were brought into a range between 0 and 1 by min–max normalization. This step has ensured that the inputs fell in comparable ranges and had similar dynamic properties for effective integration while calculating the Hybrid Vegetation Index, HVI, and onwards. The integration of radar and optical data by applying such normalizing processes allowed physical consistency for complete integration without losing the characteristics of each sensor.

$$\textbf{Linear Value} = 10^{(\mathrm{dB}/10)} \tag{1}$$

However, ensuring the consistent spatial resolution of S-1, S-2, and Landsat-8 datasets was problematic since their native resolutions differ.

S-1 radar data have a 10-m spatial resolution, while S-2 optical bands have 10 m in the visible and near-infrared parts of the spectrum, and 20 m in the shortwave infrared part; Landsat-8 spectral bands are coarser and have a 30-m resolution. All datasets were then resampled to a common resolution of 10 m using nearest neighbor interpolation to address these discrepancies (Cao et al., 2024; Palagiri & Pal, 2024; Schwartz et al., 2022). The temporal resolution was homogenized to the coarsest revisit of the datasets, using a combination of Landsat-8 scenes for this purpose. S-1 and S-2 data in the 16-day window are composited by taking the average, which maintains coherence with minimal information gaps (Shrestha et al., 2009; Zeng et al., 2021).

Novel Hybrid Vegetation Index (HVI)

We present the Novel Hybrid Vegetation Index, which is created by merging S-1 and S-2 data. Because HVI integrates optical data from S-2 and SAR data from S-1, it has significant advantages over the Normalized Difference Vegetation Index (NDVI).

While SAR data from S-1 can pierce clouds and offer information about vegetation water content and structure, optical data from S-2 is sensitive to vegetation changes in color and structure (Mandal et al., 2020; Vijayasekaran, 2019). Equation (2) introduced a Novel Hybrid Vegetation Index (HVI) by utilizing the optical bands from S-2 bands and the dual-pol (VV-VH) Sentinel-1 SAR data.

$$\mathbf{HVI} = \frac{(\mathbf{NIR} + \mathbf{VV}) - (\mathbf{Red} + \mathbf{VH})}{(\mathbf{NIR} + \mathbf{VV}) + (\mathbf{Red} + \mathbf{VH})} \quad (2)$$

Near-infrared radiation (NIR) is sensitive to chlorophyll in plants. High NIR levels signify robust and healthy plants. Red is sensitive to chlorophyll absorption (Liu et al., 2020; Xue & Su, 2017). VH (Vertical transmit, Horizontal receive) and VV (Vertical transmit, Vertical receive) represent the radar backscatter signal in the vertical polarization and horizontal polarization respectively. It is particularly sensitive to vegetation structure and water content (Chen et al., 2020; Vreugdenhil et al., 2018). Validation of HVI was conducted using the correlation coefficient with the NDVI.

Vegetation indices calculations

Normalized Difference Vegetation Index (NDVI)

The most used metric for tracking vegetation is the NDVI (Al-Quraishi et al., 2021). Based on the plant structure's ability to absorb red light and the leaf's mesophyll layers' ability to reflect near-infrared light, the NDVI is calculated. The NDVI is highly impacted by the weather, with arid and semi-arid regions being more affected than other places (Sardooi et al., 2021). An important measure for assessing the greenness of the vegetation and giving information about its condition is the normalized difference vegetation index or NDVI (De Ocampo, 2023; Huang et al., 2021). The NDVI is crucial for tracking vegetative stress and dynamics during flash droughts because it allows for quick adjustments to soil moisture and precipitation (Nguyen et al., 2023). The well-known formula Eq. (3) can be used to compute (Afshar et al., 2021; Wu et al., 2015).

$$\mathbf{NDVI} = \frac{(\mathbf{NIR} - \mathbf{RED})}{(\mathbf{NIR} + \mathbf{RED})} \quad (3)$$

Where NIR is the near-infrared band and RED is the red band.

Soil Adjusted Vegetation Index (SAVI)

Spectral signatures of different forms of land cover are not the same as those of soil. Reflectance rises in direct proportion to wavelength increases in the visible and near-infrared regions. Nonetheless, a number of factors influence the rate of increase. The reflectance of soil can be reduced by both soil moisture and organic materials. For a variety of soil types and physiognomies, the relationship between near-infrared and red reflectance is consistent. The two values are connected and exhibit a linear connection with changes in the moisture content (Binte Mostafiz et al., 2021; Konno & Homma, 2023; Rhyma et al., 2020). For every kind of soil, there is a unique relationship. To take into consideration the impact of soil brightness in areas with a restricted amount of vegetation, the L coefficient (which is assumed in this work to be equal to 0.5) is added to the computation of SAVI, which is determined using formula Eq. 4 from NIR and RED (González-Gómez et al., 2022; Huete, 1988).

$$\mathbf{SAVI} = \frac{(\mathbf{NIR} - \mathbf{RED})}{(\mathbf{NIR} + \mathbf{RED} + \mathbf{L})} * (\mathbf{1} + \mathbf{L}) \quad (4)$$

Normalized Difference Infrared Index (NDII)

Using ratios of various near-infrared reflectance (NIR) and shortwave infrared reflectance (SWIR) values as defined by Eq. (5), the NDII was created (Fensholt & Sandholt, 2003; Mathivha & Mbatha, 2021).

$$\mathbf{NDII} = \frac{(\mathbf{NIR} - \mathbf{SWIR1})}{(\mathbf{NIR} + \mathbf{SWIR1})} \quad (5)$$

Owing to the leaf's high absorption, the NDII's shortwave infrared reflectance property, which is negatively correlated with leaf water content and offers further details on the water that is available for vegetation to use in the soil, can be used to both detect plant water stress and measure vegetation's water content (Mbatha & Xulu, 2018; Sriwongsitanon et al., 2016).

Vegetation Condition Index (VCI)

The resulting time series of NDVI images was used to extract VCI. Local variations in ecosystem productivity can be tracked by the VCI derived from NDVI (Felix N. Kogan, 1995a, 1995b). VCI is able to more accurately depict how drought stress affects vegetation. According to Eq. (6) (Jiao et al., 2019; Winkler et al., 2017), VCI is defined as follows.

$$\mathbf{VCI} = \frac{(\mathbf{NDVIi} - \mathbf{NDVImin})}{(\mathbf{NDVImax} - \mathbf{NDVImin})} \quad (6)$$

NDVIi is the pixel value of the NDVI in a particular month or year, whereas NDVI max and NDVI min are the absolute maximum and lowest values of the NDVI determined (Eq. 3) for each pixel in the same month or year. It provides how the environment affects vegetation and takes geographic variations into account (Qin et al., 2021; Shahzaman et al., 2021). To enhance VCI performance, we replace NDVI with HVI in Eq. (5) to be the following formula in Eq. (7).

$$\mathbf{VCI} = \frac{(\mathbf{HVIi} - \mathbf{HVImin})}{(\mathbf{HVImax} - \mathbf{HVImin})} \quad (7)$$

HVI_{max} and HVI_{min} are the absolute maximum and lowest values of the HVI computed (Eq. 2) for each pixel in the same month or year, whereas HVI_i is the HVI pixel value for that month or year.

Temperature Condition Index (TCI)

The TCI uses LST measurements and thermal remote sensing technology. It has been discovered that LST computed using thermal infrared bands, from sensors like Landsat 8, offers useful information on surface moisture conditions (Jiao et al., 2016). The VCI is widely used, and research indicates that it can be used for keeping track of vegetation changes and agricultural dryness on a continental scale (West et al., 2019). Felix N. Kogan (1995a, 1995b) developed the TCI utilizing an extensive daylight LST time series as shown in Eq. (8) and monitored agricultural drought using the maximum and minimum variations in surface temperature.

$$\mathbf{TCI} = \frac{(\mathbf{LSTmax} - \mathbf{LST})}{(\mathbf{LSTmax} - \mathbf{LSTmin})} \quad (8)$$

where land surface temperature is represented by LST as measured by a thermal sensor, and LSTmax and LSTmin stand for the highest and lowest values of LST during the duration of the study (Shahzaman et al., 2021).

Green Normalized Difference Vegetation Index (GNDVI`)

The characteristics of chlorophyll in green plants are accurately represented by the GNDVI (Lee et al., 2021). The formula in Eq. (9) (Gitelson et al., 1996; Song & Park, 2020) is used to determine the GNDVI.

$$\mathbf{GNDVI} = \frac{(\mathbf{NIR} - \mathbf{green})}{(\mathbf{NIR} + \mathbf{green})} \quad (9)$$

where Green is the Green band and RED is the red band. A reliable indicator of how well plants is photosynthesizing is the GNDVI. Higher GNDVI values result from healthier plants reflecting more in the near-infrared and less in the green. Conversely, flora that is stressed or unhealthy will reflect differently and have a lower GNDVI. This index is particularly useful in precision agriculture and drought monitoring (Dixon et al., 2021; Song & Park, 2020; Taddeo et al., 2019).

Principal Component Analysis

Principal Component Analysis (PCA) is a method of reducing dimensionality linearly that uses a series of lower-dimensional linear descriptors to cover the maximal variance of a data set (A. Farrag et al., 2020; Gaber et al., 2021; Migenda et al., 2024). There are local PCA approaches for non-linear data where the data space is divided into disjunctive sections, and PCA is used to estimate the major subspace in each region (Möller & Hoffmann, 2004; Olivieri, 2024). Previous research has effectively employed PCA-based drought indices to track drought episodes (Jiao et al., 2019; Tadesse et al., 2017). From the NDII, VCI, SAVI, GNDVI, and TCI, the primary information is extracted using the PCA approach, which also removes any relevant signals. The ERDAS IMAGEN software environment performs the major component transformation. The weights of the indices were determined automatically through the process of PCA. Contributions of each index to PC1 were derived from the eigenvector coefficients of the covariance matrix computed after the normalization of all the indices. The coefficients are considered to represent the relative importance of each index in explaining the variance captured by PC1 (Abdi & Williams, 2010; Migenda et al., 2024).

With respect to the NDII, VCI, SAVI, GNDVI, and TCI, the first principal component (PC1) comprises almost 75% of the data (Zhang et al., 2021). Hence, we have considered PC1 for the development of the ARSDI. Table 2 summarizes the calculated eigenvector coefficients for PC1.

Validation and performance assessment of ARSDI

Comparing a drought index's temporal and spatial data with other widely recognized drought indices is a frequently used method of validation (Hao & Singh, 2015; Zhou et al., 2013). ARSDI is validated against established drought indices such as the Vegetation Health Index (VHI), the Soil Moisture Condition Index (SMCI) and Standard Precipitation Index (SPI). The Vegetation Health Index (VHI) is one of the most commonly used remote sensing drought indicators (Bento et al., 2018; Hazaymeh et al., 2016; Pei et al., 2018; Shahzaman et al., 2021). Its definition is the simple average of two elements, the Vegetation Condition Index (VCI) and the Temperature Condition Index (TCI), which are obtained from data on the visual and thermal bands, respectively. (Bento et al., 2020; Qin et al., 2021).

Since a precipitation shortfall can cause a significant reduction in soil water content, soil moisture information is essential for tracking droughts (Jiao et al., 2019; L. Zhang et al., 2017a, 2017b). The Soil Moisture Condition index (SMCI) is one of the best indices for monitoring drought conditions. SMCI is considered to be the governing variable for agricultural drought (Cao et al., 2022; Jalayer et al., 2023). Like VCI, SMCI normalizes the soil moisture values (SM) in relation to the study period series' absolute maximum (SMmax) and absolute minimum (SMmin)(Li et al., 2024; Sánchez et al., 2016).

A region's probability of experiencing rainfall over a specific time period is indicated by the Standardized Precipitation Index (SPI) (Liu et al., 2021). Not only does it eliminate the temporal and spatial disparity of rainfall, but it also offers the advantages of stability and simple calculation. As noted, it is adaptive to changes in drought and suitable for monitoring of drought and evaluation of weather conditions beyond the monthly scale. In this study, rainfall data between 2000 and 2022 was accessed through NASA Prediction Of Worldwide Energy Resources (POWER) POWER | DAVe (nasa.gov) (accessed on July 5, 2024), and then, SPI was calculated using the SPI-6 package in RStudio software. SPI-6 values were computed for an extended period from 2000 to 2022, and values for the period of 2017 to 2022 were used as validation in our study.

The study evaluated the performance of five drought indices (ARSDI, NDVI (Afshar et al., 2021), SWCI (Chen et al., 2020), SIMI, and VSDI (Zhang et al., 2013)). The correlation between Soil Moisture Condition Index (SMCI) (Jalayer et al., 2023) and the other five drought indices was calculated to evaluate the performance of each other.

Table 2 Eigenvector coefficients for PC1 obtained from vegetation indices, which reflect the relative contribution of TCI, VCI, NDII, SAVI, and GNDVI in forming ARSDI

Index	TCI	VCI	NDII	SAVI	GNDVI
(Eigenvector Coefficient)	0.186	0.343	0.316	0.106	0.049

Results and discussions

Results

Vegetation indices

S-1 and S-2 data from 2017 to 2023 were used to calculate the HVI and NDVI time series using GEE for the two-study area as shown in Fig. 3. The correlation coefficient was calculated to evaluate the effectiveness of HVI in enhancing the NDVI performance in agricultural drought monitoring. The correlation between HVI and NDVI from 2017 to 2023 as shown in Table 3. Figure 4 shows the HVI and NDVI resulting images for the years of 2018, 2020, and 2022. Figures 5 and 6 show the time series charts of NDII, SAVI, GNDVI, VCI, and TCI for Egypt and Kenya.

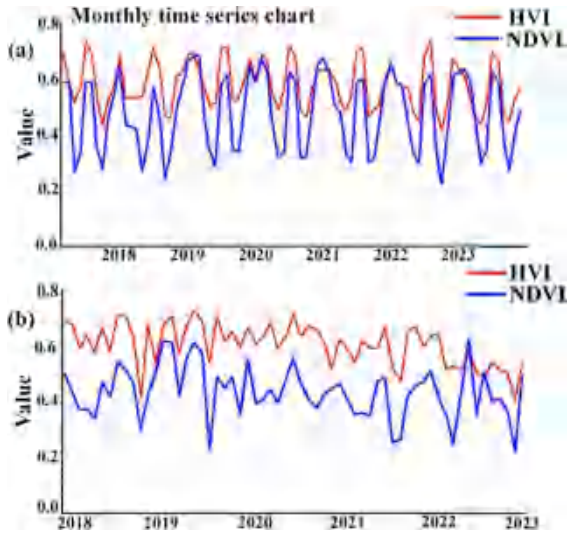

Fig. 3 Time series of HVI and NDVI for Egypt and Kenya, 2017–2023: This chart reflects the annual trend of HVI and NDVI and reflects that HVI was performing better in drought monitoring

ARSDI validation

In order to evaluate the precision of ARSDI, this study used SMCI, VHI, and SPI-6 for verification. Figures 7 and 8 illustrate the correlation between the ARSDI and SPI-6. Table 4 summarizes the correlation values between ARSDI and SPI-6. The correlation results between the ARSDI and SMCI, VHI were illustrated in Figs. 9, 10, 11, and 12. Tables 5 and 6 summarize the correlation values between ARSDI, SMCI, and VHI. The resulting drought maps for Egypt and Kenya were illustrated in Figs. 13 and 14.

Historical drought events

The validation of the Agricultural Remote Sensing Drought Index (ARSDI) was conducted by comparing it with historical drought events in Kenya and Egypt from 2017 to 2023. In Kenya, significant droughts, particularly from 2021 to 2023 (Ayugi et al., 2020; Furrer et al., 2022; King-Okumu et al., 2019; Mugabe et al., 2019; Mutsotso et al., 2018; Ochieng et al., 2022, 2023; Ondiko & Karanja, 2021; Price et al., 2022; Tanarhte et al., 2024; Uhe et al., 2018; Zhao et al., 2021), provided a valuable reference for testing ARSDI's performance. These events, characterized by failed rainy seasons and extensive agricultural loss, allowed for the assessment of ARSDI's correlation with traditional drought indicators like the Soil Moisture Condition Index (SMCI) and the Vegetation Health Index (VHI). The ARSDI demonstrated strong correlations with these indices (ranging from 0.74 to 0.85 for SMCI and 0.53 to 0.98 for VHI in Kenya), aligning closely with observed drought impacts during this period.

The correlation between Soil Moisture Condition Index (SMCI) and the other drought indices was calculated to assess how well the drought indexes performed. Tables 7 and 8 summarize the

Table 3 Correlation coefficients between HVI and NDVI for Egypt and Kenya (2017–2023) with P-value < 0.05. It shows the better performance of HVI in monitoring vegetation health and drought severity

Year Study area	2017	2018	2019	2020	2021	2022	2023
Egypt	0.90	0.93	0.95	0.95	0.94	0.93	0.93
Kenya	0.79	0.82	0.89	0.92	0.86	0.85	0.85

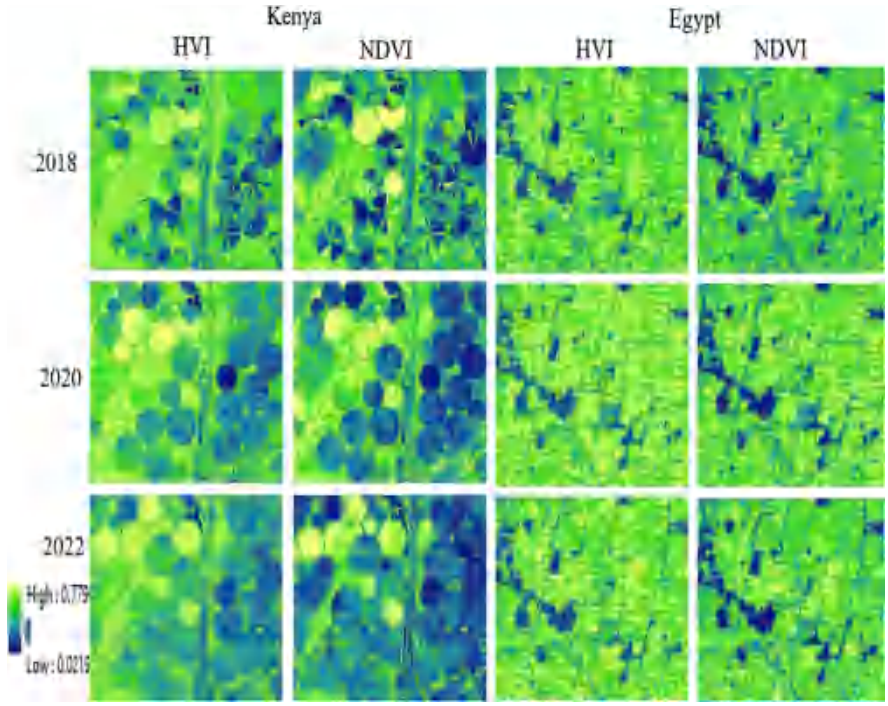

Fig. 4 Spatial distribution maps of HVI versus NDVI at Egypt and Kenya-in selected years 2018, 2020, and 2022. HVI seems to perform better in portraying vegetation health due to specific climate conditions in a more detailed manner than NDVI

correlation values between SMCI and ARSDI, NDVI, SWCI, SIMI and VSDI.

Similarly, in Egypt, ARSDI was validated against the water stress periods associated with fluctuating Nile River flows and rainfall variability (Abuhashim et al., 2021; Younes & Bakry, 2022), where it showed high correlation with SMCI (ranging from 0.64 to 0.88) and VHI (0.96 to 0.98). The accuracy of ARSDI in both countries was further reinforced by its alignment with the Standardized Precipitation Index (SPI), which ranged from 0.44 to 0.71 in Egypt and from 0.47 to 0.60 in Kenya. The integration of Sentinel-1 radar data into ARSDI allowed for more reliable vegetation and moisture monitoring, especially in regions affected by cloud cover. These validations, based on actual drought events, highlight the robustness of ARSDI in effectively capturing and analyzing drought severity in diverse environments.

Analysis of drought results

The high correlation of HVI with NDVI demonstrates a constant relationship over the years; hence, HVI would adequately replace NDVI in monitoring vegetation. Moreover, HVI has other advantages in that it makes use of S-1 SAR information; hence, data can be acquired at any time, either during the day or night and in any weather. It will, hence, promote more frequent and reliable plant monitoring, especially in areas with constant cloud cover that may hamper the performance of optical sensors like S-2. Therefore, the inclusion of radar data in HVI enhances reliability and accuracy in plant assessment, wherein it is always considered a valuable resource in carrying out rigorous drought surveillance or plant health assessment.

From the results, it is evident that ARSDI performs well in capturing drought conditions and vegetation health because it consistently shows a strong relationship with VHI in both Egypt and Kenya. In Egypt, this figure is above 0.96 for all time. Furthermore, these high correlation values in Kenya, especially between 2019 and 2022, support the accuracy of the ARSDI. The correlation between ARSDI and SPI varies across years and places from weak to substantial. In Egypt, there is a correlation from 0.44 to 0.71, while Kenya's correlation ranges from 0.47 to 0.60. These disparities suggest how complicated droughts are and how many weather elements influence SPI. Between 2018 and 2022 during the entire 6-year period, there was always a high correlation between ARSDI and SMCI, as shown by values ranging from

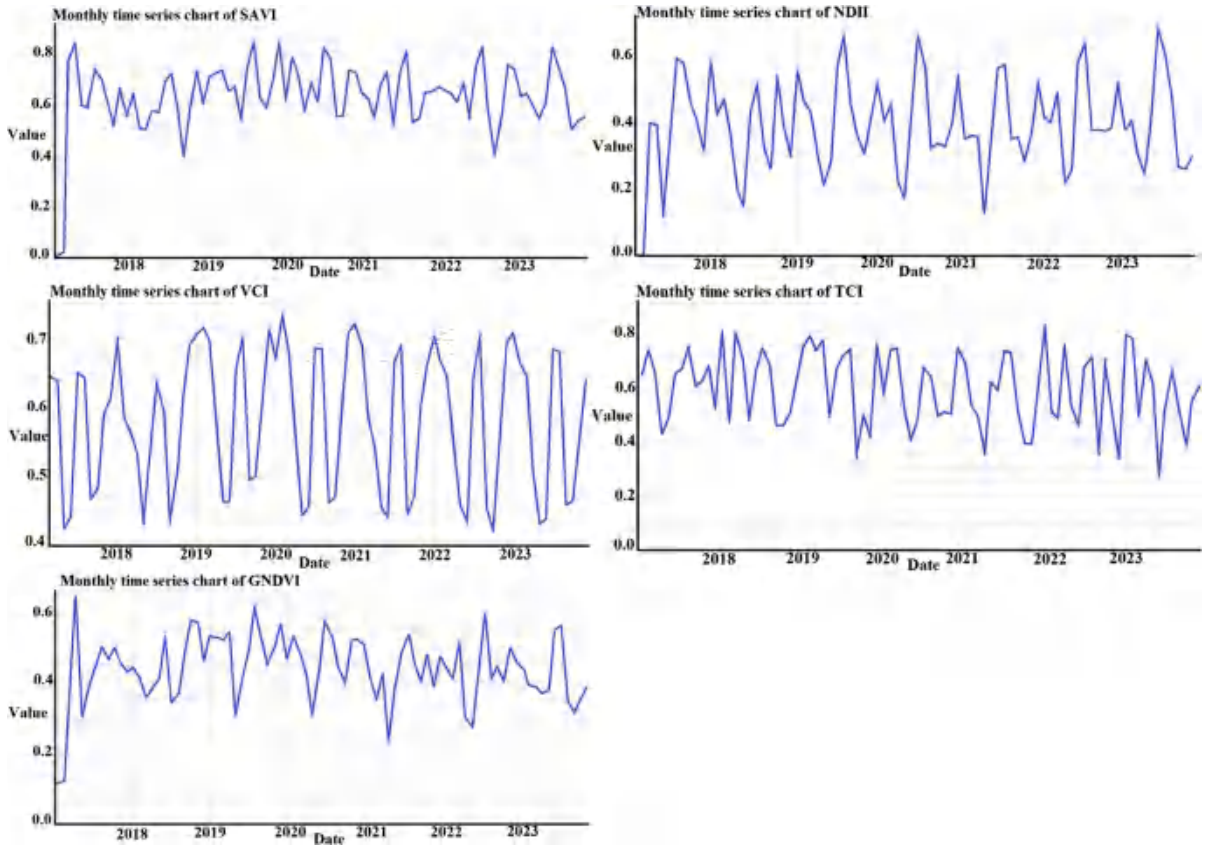

Fig. 5 Time series chart of NDII, SAVI, GNDVI, VCI, and TCI for Egypt: 2017–2023; these trends are based on different vegetation and temperature indices that show seasonal and yearly variability in reaction to climatic conditions

0.96 to 0.98 throughout Egypt. This indicates that the ARSDI can be used as a reliable index of agricultural drought related to soil moisture, specifically on variations regarding soil moisture content in a country like Egypt. This is due to the fact that Kenya has higher variability in its correlation coefficients, which range from 0.53 to 0.94 between the years of 2017 and 2019. The *P*-value is less than 0.05, indicating that our results are statistically significant.

The rise of the correlation line showing a spike at around 2021 with a value of almost one (0.96) showed that ARSDI is more efficient in representing vegetation health changes over time. However, this still indicates a strong relationship even if it slightly decreased to about 0.93 in 2022, indicating the stability of the ARSDI model when it comes to characterizing soil moisture for Kenya situations. Different types of soils, land use systems, and climatic factors could account for the uneven distribution of correlation values between Egypt and Kenya respectively. Nevertheless, these high overall correlations indicate that ARSDI is an effective tool for assessing soil moisture content under extreme drought conditions across different contextual settings.

The efficacy of the ARSADI can be determined by comparing its performance against other indices such as NDVI, SWCI, SIMI, and VSDI. In Egypt, the ARSDI and SMCI show a strong connection in 2019 and 2020 with correlations of 0.88 and 0.85, respectively. These results demonstrate the association between ARSDI and drought severity and ARSDI's efficiency in obtaining the drought magnitude data as it is superior in the dryness measurement area. The packaged ARSDI quality is also shown by the strength of the relationship of ARSDI with SMCI, which is generally higher than that of SWCI, SIMI, and VSDI. In 2022, the correlation marginally decreases to 0.64, yet it is still at a competitive level, which is a sign

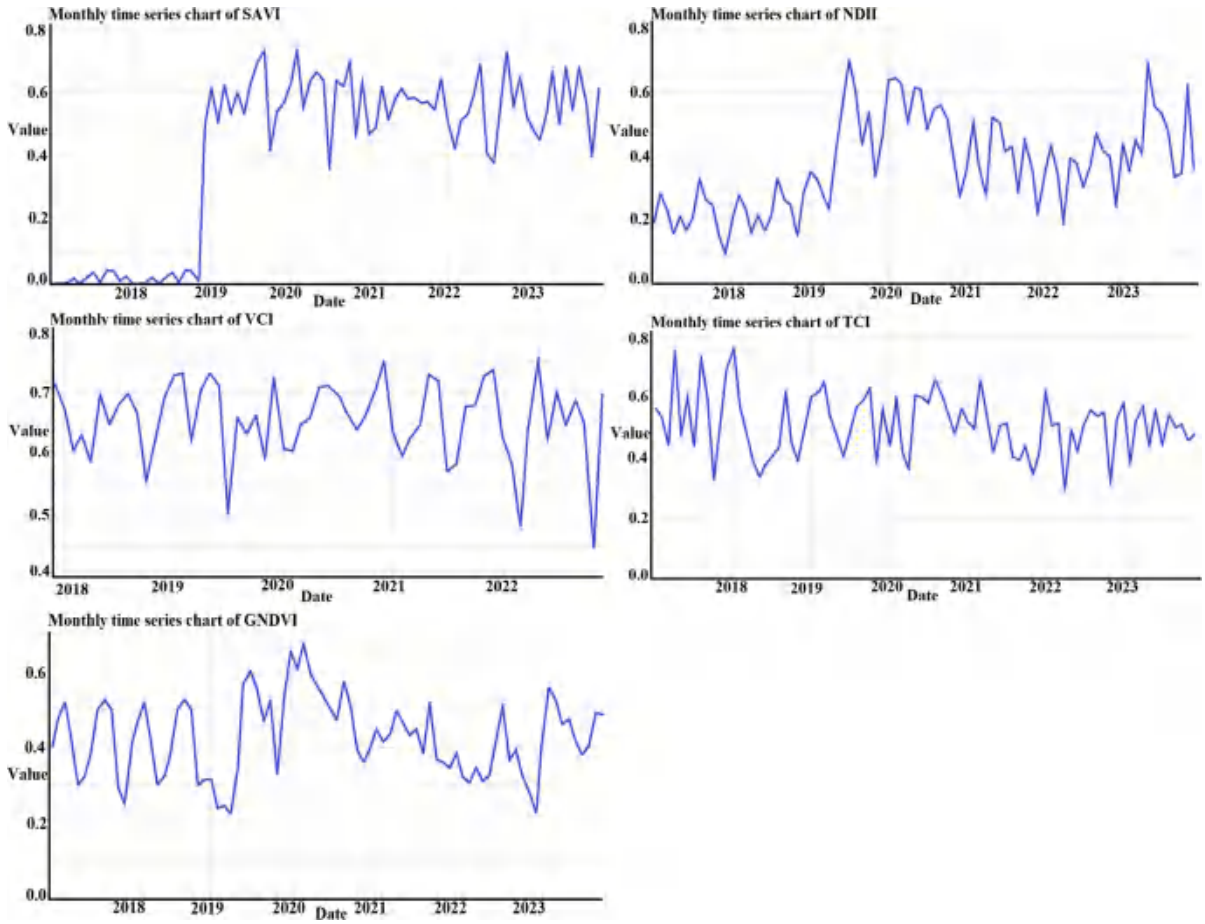

Fig. 6 Time series chart of NDII, SAVI, GNDVI, VCI, and TCI for Kenya: 2017–2023; these trends are based on different vegetation and temperature indices that show seasonal and yearly variability in reaction to climatic conditions

that it can adjust to the new weather parameters. The holistic approach of the NDVI makes it a traditional and the most effective predictor in agriculture as it shows significant correlations with SMCI, which are commonly adjacent to ARSDI. However, when one comes critically to it, ARSDI is a superior investment due to the fact that it includes in the model the mixing of the principal components PCA, and hence, it may give an explanation why it brings catchy results in specific years. ARSDI and SMCI accounted for 0.81 and 0.85 in the years 2019 and 2020 respectively. In Kenya, ARSDI and the soil moisture content index, SMCI display strong relationships again. The consistent performance of the index in various settings is a profound illustration of how good it is. Correlations in Kenya, which is a region distinguished by different soils and climates, may show unreliable relations sometimes. NDVI, as a good indicator, is still not necessarily enough to reflect the different changes in the soil moisture over time.

This conclusion comes from the parallel relationship between the vegetation index and the soil moisture in 2019 and the discrepancies in the following years.

The ARSDI seems to be the index which actually gives a more comprehensive picture in terms of evaluating drought conditions since we can observe that it consistently keeps its strength in the following years. While ARSDI generally performs better than SWCI, SWCI has moderate to high correlations in both regions. This suggests that the integrated method of ARSDI provides a more accurate and detailed description of soil moisture conditions.

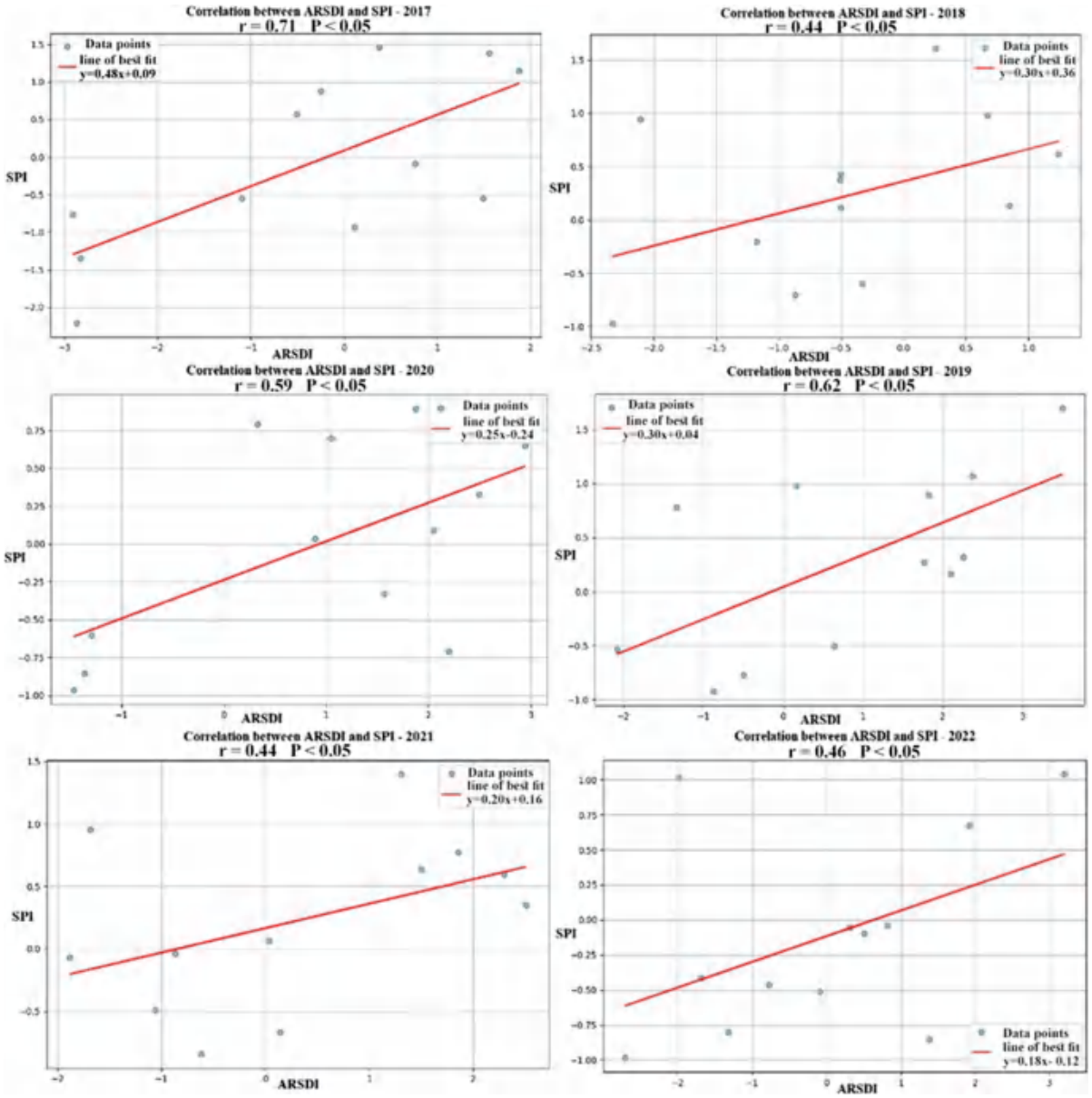

Fig. 7 Correlation of ARSDI with SPI-6 in Egypt during 2017–2022. This scatterplot indicates the statistical relation of ARSDI and Standardized Precipitation Index SPI for a period of six months

To classify the drought severity levels of the Agricultural Remote Sensing Drought Index (ARSDI), we adopted a standardized approach similar to widely used indices like the Standardized Precipitation Index (SPI) and Standardized Precipitation Evapotranspiration Index (SPEI).

Specifically, ARSDI values were standardized by calculating their deviation from the long-term mean and expressing these deviations in terms of standard deviations. Drought severity was then classified as follows: very wet for ARSDI values between + 1.50 and + 2.00 standard deviations. Mild wet ARSDI values are between + 0.50 and + 1.50 standard deviations. No drought for ARSDI values within + 0.5 and − 0.5, mild drought between − 0.5 and − 1.5, severe drought between − 1.5 and − 2.0. This method allows ARSDI

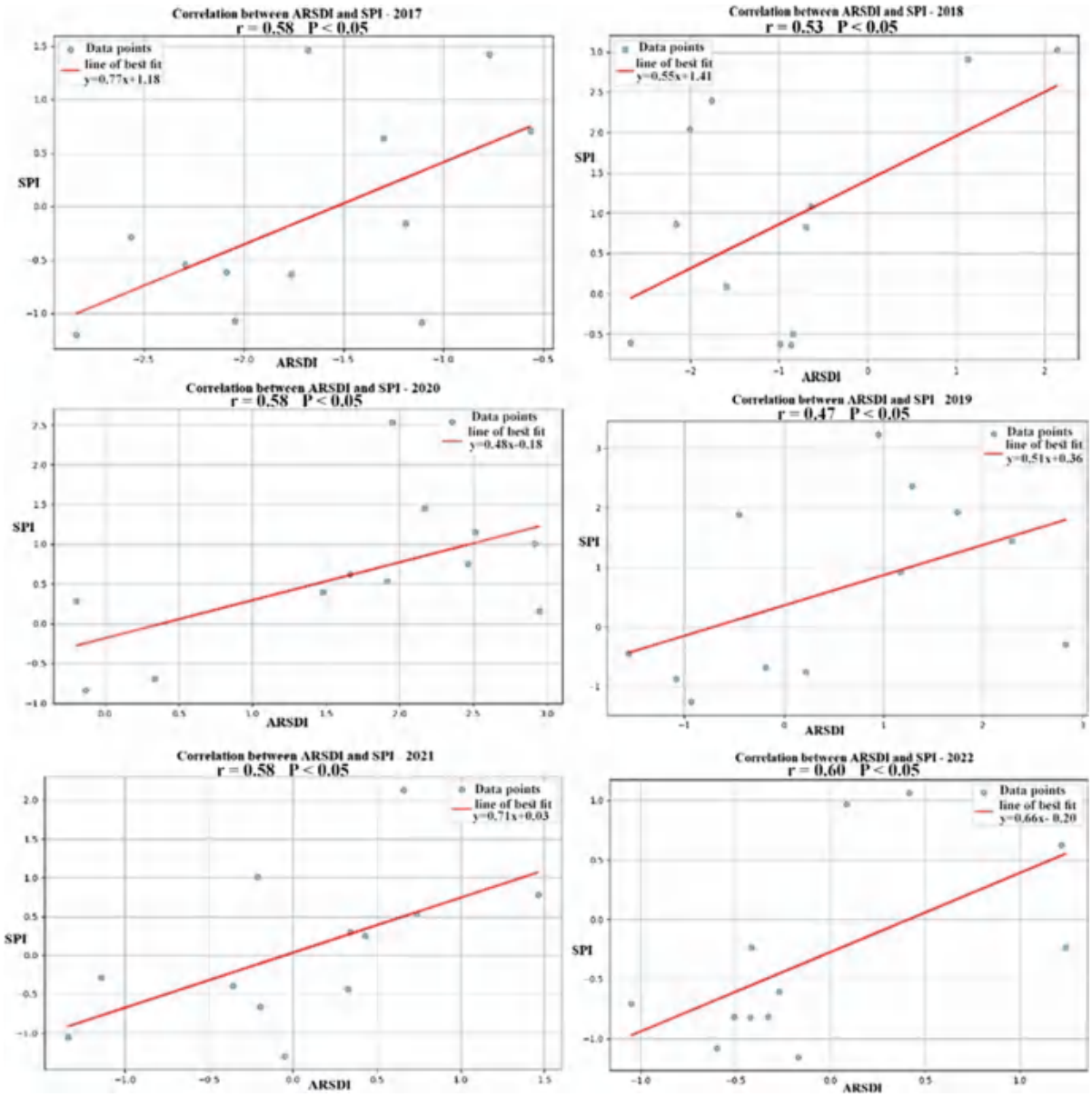

Fig. 8 Correlation of ARSDI with SPI-6 in Kenya during 2017–2022. This scatterplot indicates the statistical relation of ARSDI and Standardized Precipitation Index SPI for a period of six months

Table 4 Values of correlation coefficient between ARSDI and SPI-6 for Egypt and Kenya during 2017–2022. Results confirm the validity of ARSDI in reflecting precipitation anomalies at different time scales

Year Study area	2017	2018	2019	2020	2021	2022
Egypt	0.71	0.44	0.62	0.59	0.44	0.46
Kenya	0.58	0.53	0.47	0.58	0.58	0.60

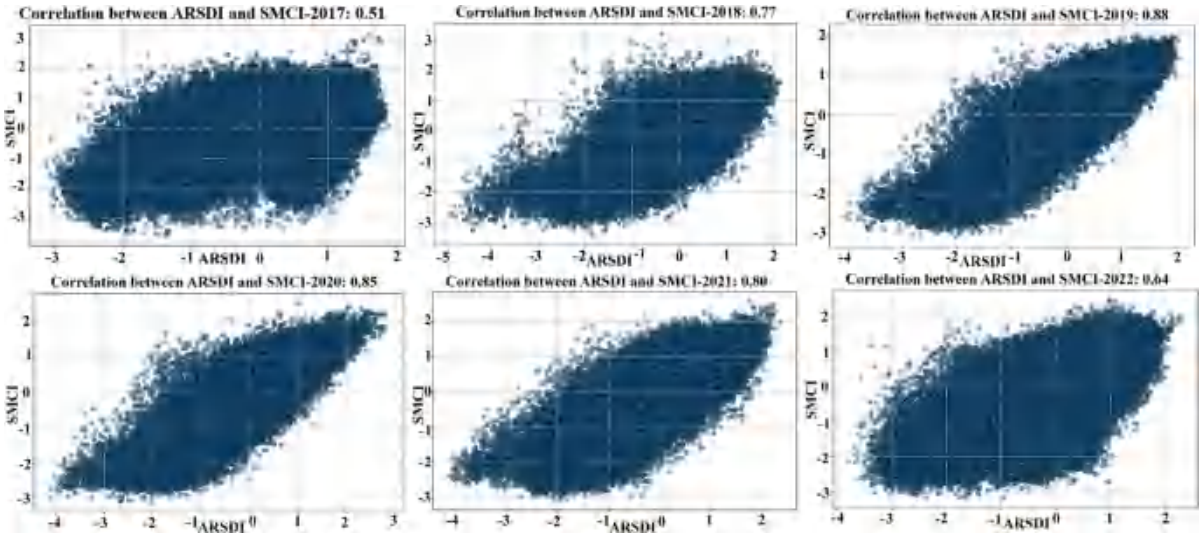

Fig. 9 Correlation between ARSDI and SMCI over Egypt for 2017–2022 with P-value < 0.05. Strong positive values are indicative of the reliability of ARSDI in capturing the variability of soil moisture under drought conditions

to capture region-specific drought conditions while accounting for natural variability in the environmental factors influencing drought. The classification was validated by correlating ARSDI with established drought indices such as the Vegetation Health Index (VHI), Soil Moisture Condition Index (SMCI), and Standardized Precipitation Index (SPI), following the approach used in the U.S. Drought Monitor and other multi-indicator frameworks (Bayissa et al., 2018; Hao & Singh, 2015; Mishra & Singh, 2010; Vicente-Serrano et al., 2010).

Discussion

The results of the study make a case for the Agricultural Remote Sensing Drought Index as a practical tool in producing correct and relatively successful drought monitoring. In this regard, ARSDI is derived by fusing S-1, S-2, and Landsat 8 data to offer an integrated drought estimate for various geographies and climatic variables, with a focus on Egypt and Kenya. Within the period from 2017 to 2022, the values of the correlation coefficient are within 0.9 to 0.95 between the Hybrid Vegetation Index and the Normalized Difference Vegetation Index. This clearly portrays that HVI can be used as a very good substitute for NDVI. In measuring HVI, S-1 uses radar data, which is totally independent of cloud cover, hence enhancing accuracy in vegetation monitoring. This suggests that, across regions that are frequently covered by cloud, increased record availability through stepped forward may be an additional advantage of adopting HVI for drought monitoring. Principal Component Analysis was next applied to determine the ARSDI after the VCI, TCI, NDII, SAVI, and GNDVI values for the study areas had been computed. This index is designed to extract the most important information from the input indices in order to give an overall view of the situation regarding drought.

The significant relationships that ARSDI has with the traditional drought indicators (VHI, SMCI, and SPI) provide more evidence of its effectiveness. Egypt's ARSDI showed correlations with VHI of 0.96 to 0.97 and SPI of 0.71 to 0.46 between 2017 and 2022. Kenya's ARSDI is similarly associated with SPI by 0.58 to 0.6 and with VHI by 0.53 to 0.93 over the same time period. These results demonstrate the ARSDI's robustness in identifying changes in soil moisture and vegetative health, two essential components of accurate drought monitoring. Compared with other indices such as NDVI, SIMI, SWCI, and VSDI, ARSDI performed best in both study areas. In Egypt, SMCI was more correlated with ARSDI (0.77–0.82) than for NDVI (0.76 to 0.84), SWCI (0.56 to 0.69), SIMI (0.19 to 0.33),

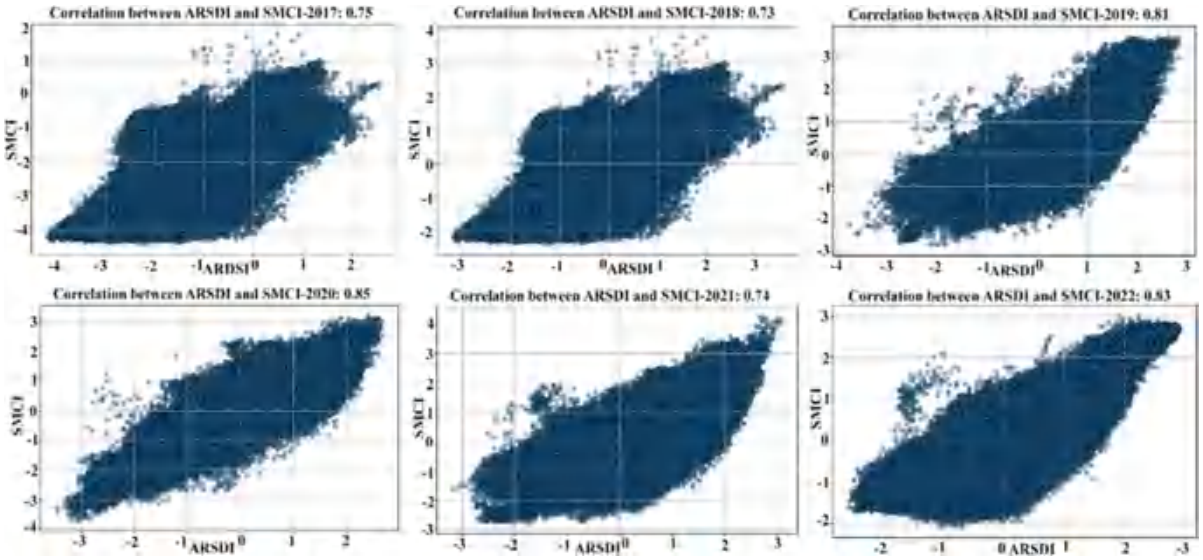

Fig. 10 Correlation between ARSDI and SMCI over Kenya for 2017–2022 with *P*-value < 0.05. Strong positive values are indicative of the reliability of ARSDI in capturing the variability of soil moisture under drought conditions

and VSDI (0.28 to 0.41) between 2019 and 2023. Similarly, Kenya had better correlations for ARSDI with SMCI (0.74–0.85) compared to those of NDVI (0.54–0.78), SWCI (0.52–0.83), SIMI (0.18–0.4), and VSDI (0.18–0.61) between the years from 2019 to 2023. These comparisons underline the strengths of using a complex index like ARSDI that combines different data sources, thus giving detailed information about drought conditions. Development and validation of ARSDI have been seen as an important advancement in monitoring droughts quantitatively. The use of virtual high-resolution data through PCA combining S-1, S-2, and landsat8 helps provide timely information on drought. When it comes to Africa, where water scarcity is a concern together with agriculture, this could be critical.

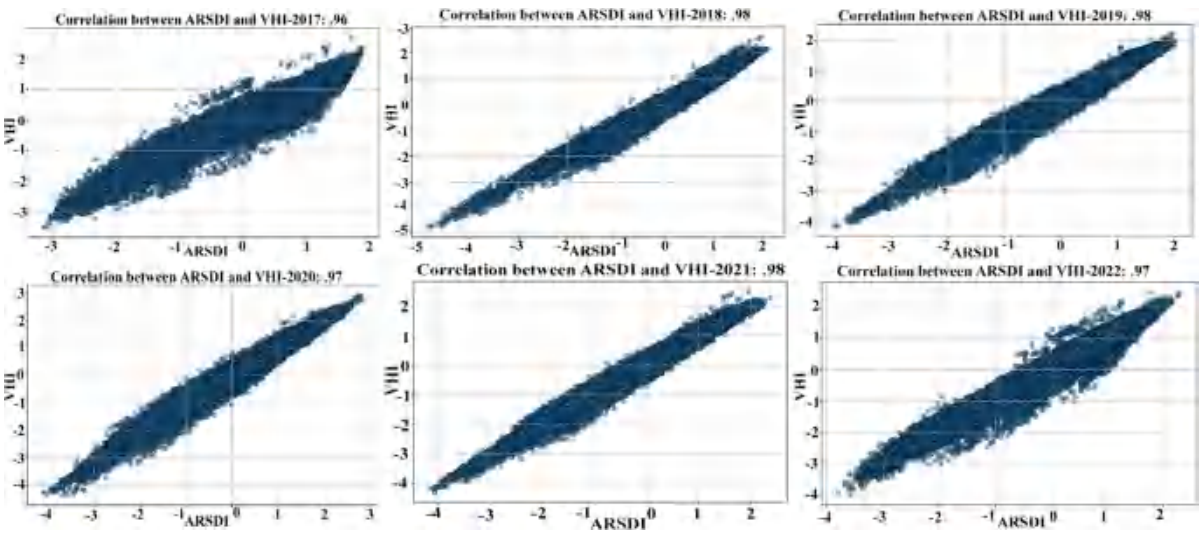

Fig. 11 Correlation between ARSDI and VHI over Egypt during the years 2017–2022 with *P*-value < 0.05: these continuous high correlations prove ARSDI performance to identify the vegetation health within the arid agriculture zones

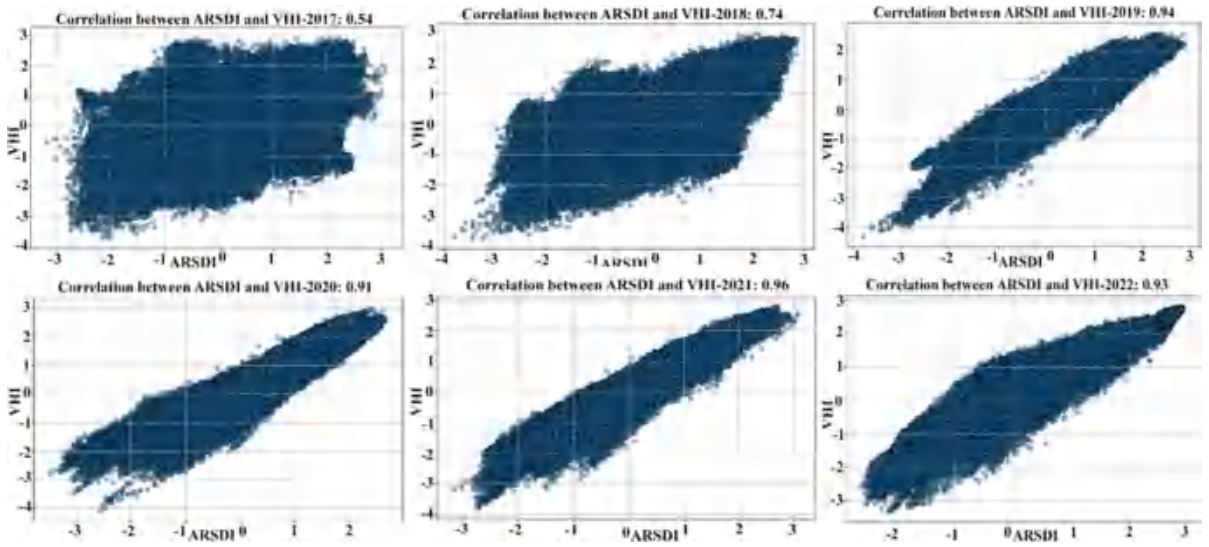

Fig. 12 Correlation between ARSDI and VHI over Kenya during the years 2017–2022 with P-value < 0.05: these continuous high correlations prove ARSDI performance to identify the vegetation health within the arid agriculture zones

Table 5 Correlation values between ARSDI and SMCI for Egypt and Kenya (2017–2023). These values highlight the strength of ARSDI in capturing soil moisture variability during drought events

Year Study area	2017	2018	2019	2020	2021	2022	2023
Egypt	0.51	0.77	0.88	0.85	0.80	0.64	0.82
Kenya	0.75	0.73	0.81	0.85	0.74	0.83	0.74

ARSDI is indeed very adaptable for regions with different climatic and agricultural practices since it uses globally available remote sensing datasets and a very flexible methodology. Employment of PCA dynamically changes the weights of the input indices according to their statistical significance, enabling ARSDI to take into consideration regional variation in vegetation, soil, and climate. Furthermore, the involved indices in ARSDI are universally applicable for monitoring drought stress, and the method allows for calibration and validation to be done with region-specific ground-truth data.

Minor modifications to this methodology may thus allow its application in regions of varied environmental conditions; for instance, a mere readjustment in weights of PCA or an addition to more evapotranspiration or water body condition-representative indices.

In some cases, ARSDI's performance was comparable or slightly inferior to classical indices such as NDVI and SPI, especially in transitions

Table 6 The ARSDI versus VHI for Egypt and Kenya during 2017–2023. This strong correlation illustrates the capability of the ARSDI in vegetation health monitoring due to drought

Year Study area	2017	2018	2019	2020	2021	2022	2023
Egypt	0.96	0.98	0.98	0.97	0.98	0.97	0.98
Kenya	0.54	0.74	0.94	0.91	0.96	0.93	0.98

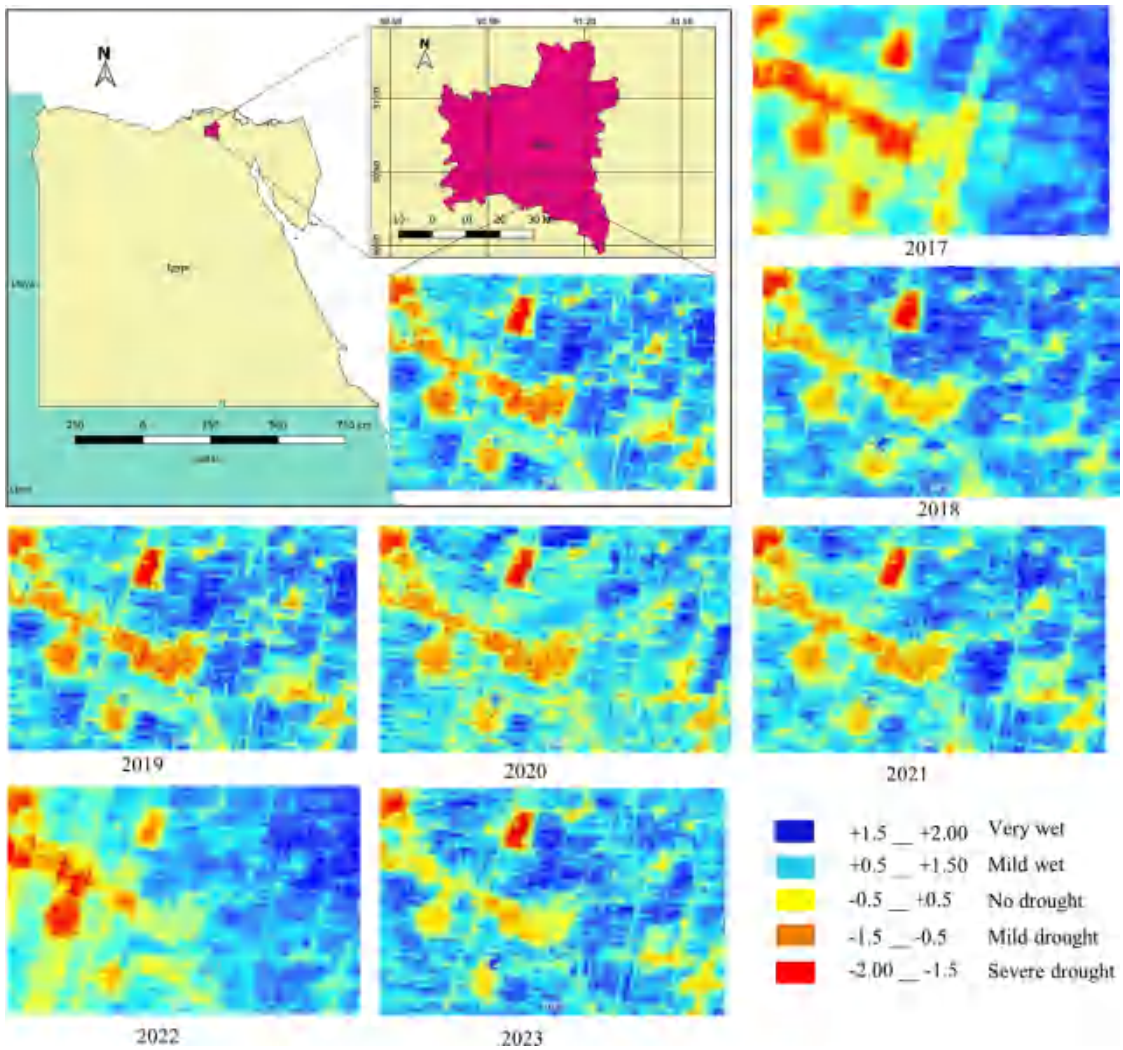

Fig. 13 ARSDI-based drought severity maps for Egypt over 2017–2023. This is a visual presentation of annual drought impacts across the Nile Delta and Valley

from extreme weather events in a short period of time, for example, from floods to droughts. Those were linked to the mismatch in temporal resolution of input datasets and the compositing nature of ARSDI, where specific responses may be diluted by such compositing.

The ability of ARSDI to integrate various environmental parameters leads to comprehensive understanding of drought conditions, thus informing better resource management decisions including policymaking. ARSDI has indeed shown good performance, but further research is required to make it more precise and effective. Expanding the validation to include other regions with diverse climatic profiles may aid in evaluating its generalization ability. Additionally, the accuracy of this index and its suitability could be improved by including such other relevant data sources as socio-economic variables and measurements of the moisture content of soil in the field. For example, the use of machine learning methods in optimizing multi-source integration and improving forecasting capabilities can be explored in future investigations for ARSDI.

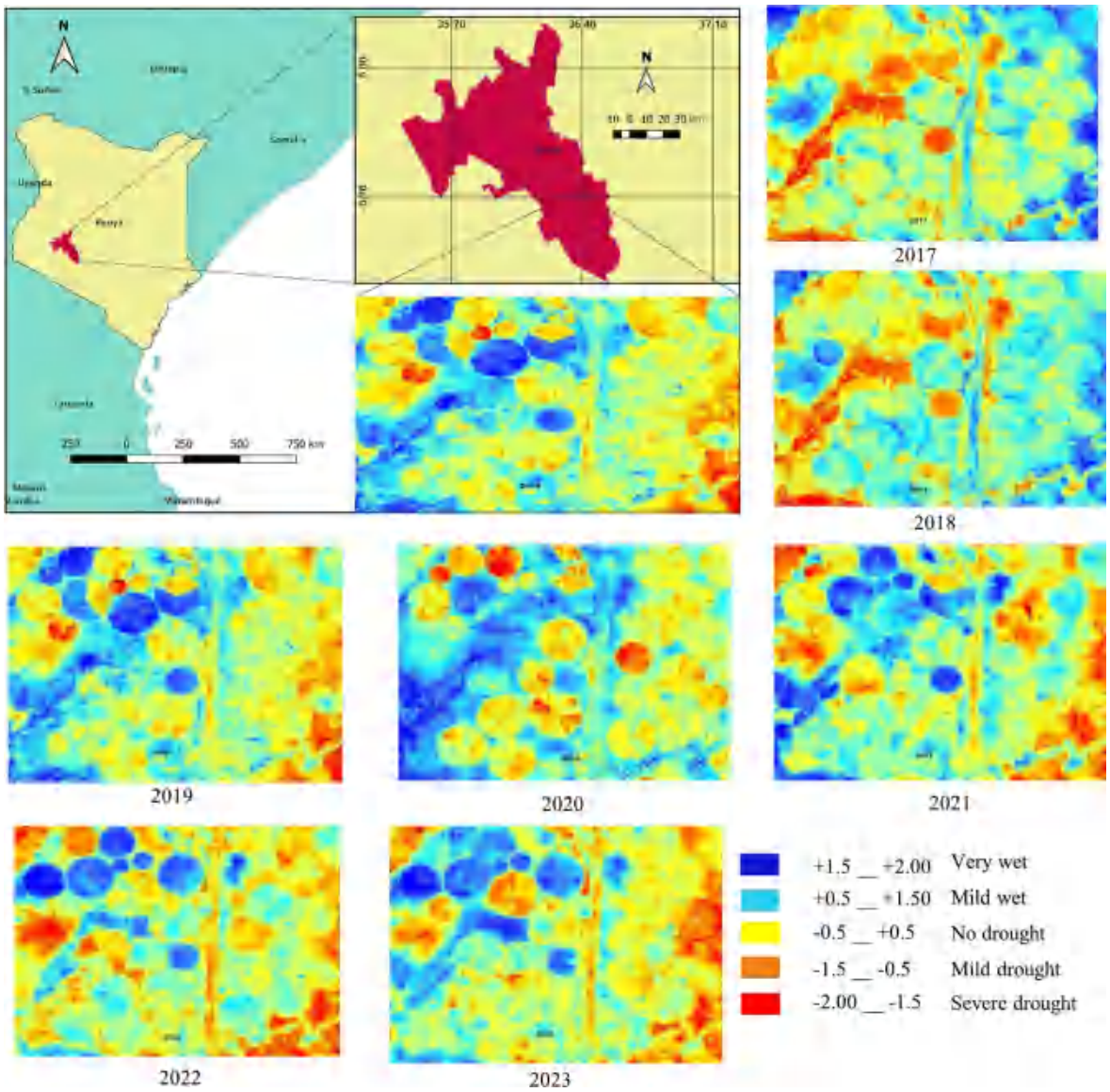

Fig. 14 ARSDI-based drought severity maps for Kenya over 2017–2023. The spatial patterns show the intensity and extent of drought across diverse agroecological zones

Conclusion

The Agricultural Remote Sensing Drought Index (ARSDI) is an innovation that has emerged from the scheme that employs data from S-1, S-2, and Landsat 8, stretching from 2017 to 2023, whose version has been validated. This assessment has been reached by combining different drought-related indices by Principal Component Analysis (PCA) and the subsequent ARSDI generations, which offer a possibly extensive view of drought conditions. The tool has undergone extensive examination in Egypt and Kenya, showing positive correlations with traditional approaches to drought, like the Vegetation Health Index (VHI), Soil moisture condition index (SMCI), and the Standardized Precipitation Index (SPI). The research revealed that the ARSDI index is always better than all other reference indices such as NDVI, SWCI, SIMI, and VSDI, which are completely insensitive to the situation. Furthermore, one of the greatest strengths of

Table 7 Performance comparison of ARSDI, NDVI, SWCI, SIMI, and VSDI over Egypt during the period 2019–2023 in relation to SMCI. ARSDI shows superiority in capturing variability in soil moisture

Year Index	2019	2020	2021	2022	2023
ARSDI	0.88	0.85	0.80	0.64	0.82
NDVI	0.85	0.83	0.81	0.84	0.8
SWCI	0.76	0.72	0.7	0.68	0.69
SIMI	0.36	0.3	0.3	0.28	0.33
VSDI	0.44	0.32	0.42	0.33	0.41

Table 8 Performance comparison of ARSDI, NDVI, SWCI, SIMI, and VSDI over Kenya, using SMCI for correlation, for the period 2019–2023. It indicates the adaptability of ARSDI to diverse climatic conditions

Year Index	2019	2020	2021	2022	2023
ARSDI	0.81	0.85	0.74	0.83	0.74
NDVI	0.78	0.75	0.57	0.54	0.71
SWCI	0.67	0.83	0.52	0.65	0.66
SIMI	0.37	0.26	0.18	0.29	0.4
VSDI	0.32	0.18	0.45	0.61	0.36

ARSDI is its near-perfect correlation with NDVI. For instance, there is a high level of correlation between NDVI and ARSDI ($R = 0.9$ to 0.95) but at the same time, the high degree in both Egypt and Kenya (the range of correlations is from 0.71 to 0.46 for SPI and 0.96 to 0.97 for VHI in Egypt, and from 0.58 to 0.6 for SPI and 0.53 to 0.93 for VHI in Kenya) become evidence to the immunity and stability of ARSDI. The implications of this study pointed towards the advantages of utilizing high-resolution, multi-sensor data for drought monitoring. It is proved that the integration of Sentinel-1 radar data, which is not affected by cloudy weather, into the ARSDI enhances the performance of the index, which makes it a particularly useful tool in areas prone to cloud formation. The strength of ARSDI to bring together the different environmental parameters guarantees a detailed and timely understanding of the status of drought, which is ace in effective resource management in the policymaking process. Besides, the excellent efficacy of ARSDI as opposed to traditional indexes implies its wider usage in a multitude of different situations. This is mainly true in areas like Africa, for example, where such issues as water shortage and agricultural production are most critical. The research also highlights the necessity for further studies in order to revise the index, approve the validity of it through various climatic regions, and search for the application of more datasets and machine learning algorithms to forecast its predictive power. The ARSDI may be regarded as an excellent breakthrough in the field of drought management as it presents a trustworthy, high-resolution instrument for drought evaluation. Its production and verification represent the direction we must go in to make our agriculture more resistant to drought and manage our resources in risky areas, specifically dealing with problems of climate change and scarcity of water.

Author contribution Nasser.A.M. Abdelrahim: Conceived the idea, conducted the research, research work, conducted the research, and write-up the manuscript. Shuanggen Jin: Helped in research work, edited the manuscript and reviewed the manuscript.

Funding This work was supported by the Henan International Science and Technology Cooperation Key Project (Grant No. 241111520700), Henan Department of Education's "Double First-Class" Project (Grant No. 760507/033) and Henan Polytechnic University Startup Foundation Project (Grant No. 722403/067/002).

Data availability Satellite scenes were accessed and processed within the Google Earth Engine environment (https://earthengine.google.com/).

Declarations

Ethical approval All the authors have read, understood, and have complied as applicable with the statement on "Ethical responsibilities of Authors" as found in the Instructions for Authors.

Competing interests The authors declare no competing interests.

References

Abdi, A. M. (2020). Land cover and land use classification performance of machine learning algorithms in a boreal landscape using Sentinel-2 data. *Giscience & Remote Sensing, 57*, 1–20. https://doi.org/10.1080/15481603.2019.1650447

Abdi, H., & Williams, L. J. (2010). Principal Component Analysis. *Wires Computational Stats, 2*, 433–459. https://doi.org/10.1002/wics.101

Abu-hashim, M., Khebour Allouche, F., Negm, A. (Eds.), 2021. Agro-Environmental Sustainability in MENA Regions, Springer Water. Springer International Publishing, Cham. https://doi.org/10.1007/978-3-030-78574-1

Afshar, M. H., Al-Yaari, A., & Yilmaz, M. T. (2021). Comparative evaluation of microwave L-band VOD and optical NDVI for agriculture drought detection over Central Europe. *Remote Sensing, 13*, 1251. https://doi.org/10.3390/rs13071251

Afzal, M., & Ragab, R. (2019). Drought risk under climate and land use changes: Implication to water resource availability at catchment scale. *Water, 11*, 1790. https://doi.org/10.3390/w11091790

Alahacoon, N., & Edirisinghe, M. (2022). A comprehensive assessment of remote sensing and traditional based drought monitoring indices at global and regional scale. *Geomatics, Natural Hazards and Risk, 13*, 762–799. https://doi.org/10.1080/19475705.2022.2044394

Alahacoon, N., Edirisinghe, M., & Ranagalage, M. (2021). Satellite-based meteorological and agricultural drought monitoring for agricultural sustainability in Sri Lanka. *Sustainability, 13*, 3427. https://doi.org/10.3390/su13063427

Alito, K. T., & Kerebih, M. S. (2024). Spatio-temporal assessment of agricultural drought using remote sensing and ground-based data indices in the Northern Ethiopian Highland. *Journal of Hydrology: Regional Studies, 52*, 101700. https://doi.org/10.1016/j.ejrh.2024.101700

Alkaraki, K. F., & Hazaymeh, K. (2023). A comprehensive remote sensing-based Agriculture Drought Condition Indicator (CADCI) using machine learning. *Environmental Challenges, 11*, 100699. https://doi.org/10.1016/j.envc.2023.100699

Al-Quraishi, A. M. F., Gaznayee, H. A., & Crespi, M. (2021). Drought trend analysis in a semi-arid area of Iraq based on Normalized Difference Vegetation Index, Normalized Difference Water Index and Standardized Precipitation Index. *Journal of Arid Land, 13*, 413–430. https://doi.org/10.1007/s40333-021-0062-9

Araneda-Cabrera, R. J., Bermúdez, M., & Puertas, J. (2021). Benchmarking of drought and climate indices for agricultural drought monitoring in Argentina. *Science of the Total Environment, 790*, 148090. https://doi.org/10.1016/j.scitotenv.2021.148090

Arun Kumar, K. C., Reddy, G. P. O., Masilamani, P., Turkar, S. Y., & Sandeep, P. (2021). Integrated drought monitoring index: A tool to monitor agricultural drought by using time-series datasets of space-based earth observation satellites. *Advances in Space Research, 67*, 298–315. https://doi.org/10.1016/j.asr.2020.10.003

Atzberger, C. (2013). Advances in remote sensing of agriculture: Context description, existing operational monitoring systems and major information needs. *Remote Sensing, 5*, 949–981. https://doi.org/10.3390/rs5020949

Ayugi, B., Tan, G., Niu, R., Dong, Z., Ojara, M., Mumo, L., Babaousmail, H., & Ongoma, V. (2020). Evaluation of meteorological drought and flood scenarios over Kenya. *East Africa. Atmosphere, 11*, 307. https://doi.org/10.3390/atmos11030307

Bayissa, Y., Maskey, S., Tadesse, T., Van Andel, S., Moges, S., Van Griensven, A., & Solomatine, D. (2018). Comparison of the performance of six drought indices in characterizing historical drought for the Upper Blue Nile Basin. *Ethiopia. Geosciences, 8*, 81. https://doi.org/10.3390/geosciences8030081

Bento, V. A., Gouveia, C. M., DaCamara, C. C., & Trigo, I. F. (2018). A climatological assessment of drought impact on vegetation health index. *Agricultural and Forest Meteorology, 259*, 286–295. https://doi.org/10.1016/j.agrformet.2018.05.014

Bento, V. A., Gouveia, C. M., DaCamara, C. C., Libonati, R., & Trigo, I. F. (2020). The roles of NDVI and Land Surface Temperature when using the Vegetation Health Index over dry regions. *Global and Planetary Change, 190*, 103198. https://doi.org/10.1016/j.gloplacha.2020.103198

Bhogapurapu, N., Dey, S., Mandal, D., Bhattacharya, A., Karthikeyan, L., McNairn, H., & Rao, Y. S. (2022). Soil moisture retrieval over croplands using dual-pol L-band GRD SAR data. *Remote Sensing of Environment, 271*, 112900. https://doi.org/10.1016/j.rse.2022.112900

Bhuiyan, C., Singh, R. P., & Kogan, F. N. (2006). Monitoring drought dynamics in the Aravalli region (India) using different indices based on ground and remote sensing data. *International Journal of Applied Earth Observation and Geoinformation, 8*, 289–302. https://doi.org/10.1016/j.jag.2006.03.002

Binte Mostafiz, R., Noguchi, R., & Ahamed, T. (2021). Agricultural land suitability assessment using satellite remote sensing-derived soil-vegetation indices. *Land, 10*, 223. https://doi.org/10.3390/land10020223

Brandt, M., Hiernaux, P., Rasmussen, K., Mbow, C., Kergoat, L., Tagesson, T., Ibrahim, Y. Z., Wélé, A., Tucker, C. J., & Fensholt, R. (2016). Assessing woody vegetation trends in Sahelian drylands using MODIS based seasonal metrics. *Remote Sensing of Environment, 183*, 215–225. https://doi.org/10.1016/j.rse.2016.05.027

Braun, A., Veci, L. (2015). SAR Basics Tutorial. European Space Agency (ESA).

Cao, M., Chen, M., Liu, J., & Liu, Y. (2022). Assessing the performance of satellite soil moisture on agricultural drought monitoring in the North China Plain. *Agricultural Water Management, 263*, 107450. https://doi.org/10.1016/j.agwat.2021.107450

Cao, J., Luo, Y., Zhang, X., Fan, L., Tao, J., Nam, W.-H., Sur, C., He, Y., Gulakhmadov, A., & Niyogi, D. (2024). Assessing the responsiveness of multiple microwave remote sensing vegetation optical depth indices to drought on crops in Midwest US. *International Journal of Applied Earth Observation and Geoinformation, 132*, 104072. https://doi.org/10.1016/j.jag.2024.104072

Chen, N., Yu, L., Zhang, X., Shen, Y., Zeng, L., Hu, Q., & Niyogi, D. (2020). Mapping paddy rice fields by combining multi-temporal vegetation index and synthetic aperture radar remote sensing data using Google Earth Engine machine learning platform. *Remote Sensing, 12*, 2992. https://doi.org/10.3390/rs12182992

Corbari, C., Paciolla, N., Restuccia, G., & Al Bitar, A. (2024). Multi-scale EO-based agricultural drought monitoring indicator for operative irrigation networks management in Italy. *Journal of Hydrology: Regional Studies, 52*, 101732. https://doi.org/10.1016/j.ejrh.2024.101732

Dalezios, N. R., Blanta, A., & Spyropoulos, N. V. (2012). Assessment of remotely sensed drought features in vulnerable agriculture. *Natural Hazards and Earth Systems Sciences, 12*, 3139–3150. https://doi.org/10.5194/nhess-12-3139-2012

Dixon, D. J., Callow, J. N., Duncan, J. M. A., Setterfield, S. A., & Pauli, N. (2021). Satellite prediction of forest flowering phenology. *Remote Sensing of Environment, 255*, 112197. https://doi.org/10.1016/j.rse.2020.112197

Dong, J., Xing, L., Cui, N., Zhao, L., Guo, L., & Gong, D. (2023). Standardized precipitation evapotranspiration index (SPEI) estimated using variant long short-term memory network at four climatic zones of China. *Computers and Electronics in Agriculture, 213*, 108253. https://doi.org/10.1016/j.compag.2023.108253

Dos Santos Araujo, D. C., Gico Lima Montenegro, S. M., Ribeiro Neto, A., & Da Silva, S. F. (2024). Evaluation of satellite-based soil moisture for agricultural drought monitoring in the Brazilian semiarid region. *Remote Sensing Applications: Society and Environment, 33*, 101111. https://doi.org/10.1016/j.rsase.2023.101111

Dotzler, S., Hill, J., Buddenbaum, H., & Stoffels, J. (2015). The Potential of EnMAP and Sentinel-2 Data for Detecting Drought Stress Phenomena in Deciduous Forest Communities. *Remote Sensing, 7*, 14227–14258. https://doi.org/10.3390/rs71014227

Du, L., Tian, Q., Yu, T., Meng, Q., Jancso, T., Udvardy, P., & Huang, Y. (2013). A comprehensive drought monitoring method integrating MODIS and TRMM data. *International Journal of Applied Earth Observation and Geoinformation, 23*, 245–253. https://doi.org/10.1016/j.jag.2012.09.010

Edokossi, K., Calabia, A., Jin, S., & Molina, I. (2020). GNSS-reflectometry and remote sensing of soil moisture: A review of measurement techniques, methods, and applications. *Remote Sensing, 12*, 614. https://doi.org/10.3390/rs12040614

Edokossi, K., Jin, S., Calabia, A., Molina, I., & Mazhar, U. (2024). Evaluation of SMAP and CYGNSS soil moistures in drought prediction using multiple linear regression and GLDAS product. *Photogrammetric Engineering & Remote Sensing, 90*, 303–312.

Elameen, A. M., Jin, S., & Olago, D. (2023). Identification of drought events in major basins of Africa from GRACE total water storage and modeled products. *Photogrammetric Engineering & Remote Sensing, 89*, 221–232.

Farrag, F. A., Mostafa, Y. G., & Mohamed, N. A. (2020). Detecting land cover changes using VHR satellite images: A comparative study. *JES. Journal of Engineering Sciences, 48*, 200–211. https://doi.org/10.21608/jesaun.2019.264927

Fawzy, H.E.-D., Sakr, A., El-Enany, M., & Moghazy, H. M. (2021). Spatiotemporal assessment of actual evapotranspiration using satellite remote sensing technique in the Nile Delta. *Egypt. Alexandria Engineering Journal, 60*, 1421–1432. https://doi.org/10.1016/j.aej.2020.11.001

Felegari, S., Sharifi, A., Moravej, K., Amin, M., Golchin, A., Muzirafuti, A., Tariq, A., & Zhao, N. (2021). Integration of Sentinel 1 and Sentinel 2 Satellite Images for Crop Mapping. *Applied Sciences, 11*, 10104. https://doi.org/10.3390/app112110104

Fensholt, R., & Sandholt, I. (2003). Derivation of a shortwave infrared water stress index from MODIS near- and shortwave infrared data in a semiarid environment. *Remote Sensing of Environment, 87*, 111–121. https://doi.org/10.1016/j.rse.2003.07.002

Furrer, M., Mostofi, H., & Spinler, S. (2022). A study on the impact of extreme weather events on the ceramic manufacturing in Egypt. *Resources, Environment and Sustainability, 7*, 100049. https://doi.org/10.1016/j.resenv.2022.100049

Gaber, Y., Ahmed, N., & Ali Farrag, F. (2021). Change detection for map updating using very high resolution satellite images. *JES. Journal of Engineering Sciences, 0*, 424–445. https://doi.org/10.21608/jesaun.2021.67949.1039

Gitelson, A. A., Kaufman, Y. J., & Merzlyak, M. N. (1996). Use of a green channel in remote sensing of global vegetation from EOS-MODIS. *Remote Sensing of Environment, 58*, 289–298. https://doi.org/10.1016/S0034-4257(96)00072-7

González-Gómez, L., Intrigliolo, D. S., Rubio-Asensio, J. S., Buesa, I., & Ramírez-Cuesta, J. M. (2022). Assessing almond response to irrigation and soil management practices using vegetation indexes time-series and plant water status measurements. *Agriculture, Ecosystems & Environment, 339*, 108124. https://doi.org/10.1016/j.agee.2022.108124

Hao, Z., & Singh, V. P. (2015). Drought characterization from a multivariate perspective: A review. *Journal of Hydrology, 527*, 668–678. https://doi.org/10.1016/j.jhydrol.2015.05.031

Hayes, M. J., Svoboda, M. D., Wardlow, B. D., Anderson, M. C., Kogan, F., (n.d). Drought monitoring: Historical and current perspectives.

Hazaymeh, K., & Hassan, Q. K. (2017). A remote sensing-based agricultural drought indicator and its implementation over a semi-arid region. *Jordan. J. Arid Land, 9*, 319–330. https://doi.org/10.1007/s40333-017-0014-6

Hazaymeh, K., Hassan, K., & Q. (2016). 1 Department of Geomatics Engineering, Schulich School of Engineering, University of Calgary, 2500 University Drive NW, Calgary, Alberta, Canada T2N 1N4, 2016. Remote sensing of agricultural drought monitoring: A state of art review. *AIMS Environmental Science, 3*, 604–630. https://doi.org/10.3934/environsci.2016.4.604

Holben, B. N. (1980). Spectral assessment of soybean leaf area and leaf biomass. PHOTOGRAMMETRIC ENGINEERING.

Huang, S., Tang, L., Hupy, J. P., Wang, Y., & Shao, G. (2021). A commentary review on the use of normalized difference vegetation index (NDVI) in the era of popular remote sensing. *Journal of Forest Research, 32*, 1–6. https://doi.org/10.1007/s11676-020-01155-1

Huete, A. R. (1988). A soil-adjusted vegetation index (SAVI). *Remote Sensing of Environment, 25*, 295–309. https://doi.org/10.1016/0034-4257(88)90106-X

Jalayer, S., Sharifi, A., Abbasi-Moghadam, D., Tariq, A., & Qin, S. (2023). Assessment of spatiotemporal characteristic of droughts using *in situ* and remote sensing-based drought indices. *IEEE Journal of Selected Topics in Applied Earth Observations Remote Sensing, 16*, 1483–1502. https://doi.org/10.1109/JSTARS.2023.3237380

Jiao, W., Zhang, L., Chang, Q., Fu, D., Cen, Y., & Tong, Q. (2016). Evaluating an Enhanced Vegetation Condition Index (VCI) based on VIUPD for drought monitoring in the continental United States. *Remote Sensing, 8*, 224. https://doi.org/10.3390/rs8030224

Jiao, W., Tian, C., Chang, Q., Novick, K. A., & Wang, L. (2019). A new multi-sensor integrated index for drought monitoring. *Agricultural and Forest Meteorology, 268*, 74–85. https://doi.org/10.1016/j.agrformet.2019.01.008

Jin, S., & Zhang, T. (2016). Terrestrial water storage anomalies associated with drought in Southwestern USA from GPS Observations. *Surveys in Geophysics, 37*, 1139–1156. https://doi.org/10.1007/s10712-016-9385-z

Jin, S., Wang, Q., & Dardanelli, G. (2022). A review on multi-GNSS for Earth observation and emerging applications. *Remote Sensing, 14*, 3930. https://doi.org/10.3390/rs14163930

Jin, S., Camps, A., Jia, Y., Wang, F., Martin-Neira, M., Huang, F., Yan, Q., Zhang, S., Li, Z., Edokossi, K., Yang, D., Xiao, Z., Ma, Z., & Bai, W. (2024). Remote sensing and its applications using GNSS reflected signals: Advances and prospects. *Satell Navig, 5*, 19. https://doi.org/10.1186/s43020-024-00139-4

Kaiser, P., Buddenbaum, H., Nink, S., & Hill, J. (2022). Potential of Sentinel-1 data for spatially and temporally high-resolution detection of drought affected forest stands. *Forests, 13*, 2148. https://doi.org/10.3390/f13122148

Kaushik, P., Jabin, S. (2018). A comparative study of pre-processing techniques of SAR images, in: 2018 4th International Conference on Computing Communication and Automation (ICCCA). Presented at the 2018 4th International Conference on Computing Communication and Automation (ICCCA), IEEE, pp. 1–4. https://doi.org/10.1109/CCAA.2018.8777710

Khater, A., Kitamura, Y., Shimizu, K., Abou El Hassan, W., & Fujimaki, H. (2015). Quantitative analysis of reusing agricultural water to compensate for water supply deficiencies in the Nile Delta irrigation network. *Paddy and Water Environment, 13*, 367–378. https://doi.org/10.1007/s10333-014-0454-y

Khorrami, B., & Gunduz, O. (2020). Spatio-temporal interactions of surface urban heat island and its spectral indicators: A case study from Istanbul metropolitan area. *Turkey. Environ Monit Assess, 192*, 386. https://doi.org/10.1007/s10661-020-08322-1

Khorrami, B., & Gunduz, O. (2021). An enhanced water storage deficit index (EWSDI) for drought detection using GRACE gravity estimates. *Journal of Hydrology, 603*, 126812. https://doi.org/10.1016/j.jhydrol.2021.126812

Khorrami, B., & Gündüz, O. (2022). Detection and analysis of drought over Turkey with remote sensing and model-based drought indices. *Geocarto International, 37*, 12171–12193. https://doi.org/10.1080/10106049.2022.2066197

Khorrami, B., Ali, S., & Gündüz, O. (2023). An appraisal of the local-scale spatio-temporal variations of drought based on the integrated GRACE / GRACE-FO observations and fine-resolution FLDAS model. *Hydrological Processes, 37*, e15034. https://doi.org/10.1002/hyp.15034

King-Okumu, C., Orindi, V.A., Lekalkuli, L. (2019). Drought management in the drylands of Kenya: what have we learned?, in: Current directions in water scarcity research. Elsevier, pp. 277–294. https://doi.org/10.1016/B978-0-12-814820-4.00019-5

Kogan, F. N. (1995a). Droughts of the Late 1980s in the United States as Derived from NOAA Polar-Orbiting Satellite Data. *Bull. Amer. Meteor. Soc., 76*, 655–668. https://doi.org/10.1175/1520-0477(1995)076%3c0655:DOTLIT%3e2.0.CO;2

Kogan, F. N. (1995b). Application of vegetation index and brightness temperature for drought detection. *Advances in Space Research, 15*, 91–100. https://doi.org/10.1016/0273-1177(95)00079-T

Kogan, F. N. (1997). Global Drought Watch from Space. *Bull. Amer. Meteor. Soc., 78*, 621–636. https://doi.org/10.1175/1520-0477(1997)078%3c0621:GDWFS%3e2.0.CO;2

Konno, T., & Homma, K. (2023). Prediction of areal soybean lodging using a main stem elongation model and a soil-adjusted vegetation index that accounts for the ratio of vegetation cover. *Remote Sensing, 15*, 3446. https://doi.org/10.3390/rs15133446

Kulkarni, S. S., Wardlow, B. D., Bayissa, Y. A., Tadesse, T., Svoboda, M. D., & Gedam, S. S. (2020). Developing a remote sensing-based combined drought indicator approach for agricultural drought monitoring over Marathwada. *India. Remote Sensing, 12*, 2091. https://doi.org/10.3390/rs12132091

Kumari, A., & Karthikeyan, S. (2023). Sentinel-2 Data for Land Use/Land Cover Mapping: A Meta-analysis and Review. *SN COMPUT. SCI., 4*, 815. https://doi.org/10.1007/s42979-023-02214-0

Lee, G., Hwang, J., & Cho, S. (2021). A novel index to detect vegetation in urban areas using UAV-based multispectral images. *Applied Sciences, 11*, 3472. https://doi.org/10.3390/app11083472

Li, L., & Cai, H. (2024). A comparative study of various drought indices at different timescales and over different record lengths in the arid area of northwest China. *Environmental Science and Pollution Research, 31*, 25096–25113. https://doi.org/10.1007/s11356-024-32803-2

Li, H., Yin, Y., Zhou, J., & Li, F. (2024). Improved agricultural drought monitoring with an integrated drought condition index in Xinjiang. *China. Water, 16*, 325. https://doi.org/10.3390/w16020325

Liu, L., Xiao, X., Qin, Y., Wang, J., Xu, X., Hu, Y., & Qiao, Z. (2020). Mapping cropping intensity in China using time series Landsat and Sentinel-2 images and Google Earth Engine. *Remote Sensing of Environment, 239*, 111624. https://doi.org/10.1016/j.rse.2019.111624

Liu, C., Yang, C., Yang, Q., & Wang, J. (2021). Spatiotemporal drought analysis by the standardized precipitation index (SPI) and standardized precipitation evapotranspiration index (SPEI) in Sichuan Province. *China. Sci Rep, 11*, 1280. https://doi.org/10.1038/s41598-020-80527-3

Malakar, N. K., & Hulley, G. C. (2016). A water vapor scaling model for improved land surface temperature and emissivity separation of MODIS thermal infrared data. *Remote Sensing of Environment, 182*, 252–264. https://doi.org/10.1016/j.rse.2016.04.023

Mancino, G., Ferrara, A., Padula, A., & Nolè, A. (2020). Cross-comparison between Landsat 8 (OLI) and Landsat 7 (ETM+) derived vegetation indices in a Mediterranean

environment. *Remote Sensing, 12*, 291. https://doi.org/10.3390/rs12020291

Mandal, D., Kumar, V., Ratha, D., Dey, S., Bhattacharya, A., Lopez-Sanchez, J. M., McNairn, H., & Rao, Y. S. (2020). Dual polarimetric radar vegetation index for crop growth monitoring using sentinel-1 SAR data. *Remote Sensing of Environment, 247*, 111954. https://doi.org/10.1016/j.rse.2020.111954

Masinde, M. (2015). An innovative drought early warning system for sub-Saharan Africa: Integrating modern and indigenous approaches. *African Journal of Science, Technology, Innovation and Development, 7*, 8–25. https://doi.org/10.1080/20421338.2014.971558

Mathivha, F., & Mbatha, N. (2021). Comparison of long-term changes in non-linear aggregated drought index calibrated by MERRA–2 and NDII soil moisture proxies. *Water, 14*, 26. https://doi.org/10.3390/w14010026

Maulana, J., & Bioresita, F. (2023). Monitoring of land surface temperature in Surabaya, Indonesia from 2013–2021 Using Landsat-8 Imagery and Google Earth Engine. *IOP Conference Series: Earth Environmental Science, 1127*, 012027. https://doi.org/10.1088/1755-1315/1127/1/012027

Mbatha, N., & Xulu, S. (2018). Time Series Analysis of MODIS-Derived NDVI for the Hluhluwe-Imfolozi Park, South Africa: Impact of Recent Intense Drought. *Climate, 6*, 95. https://doi.org/10.3390/cli6040095

Migenda, N., Möller, R., & Schenck, W. (2024). Adaptive local principal component analysis improves the clustering of high-dimensional data. *Pattern Recognition, 146*, 110030. https://doi.org/10.1016/j.patcog.2023.110030

Mishra, A. K., & Singh, V. P. (2010). A review of drought concepts. *Journal of Hydrology, 391*, 202–216. https://doi.org/10.1016/j.jhydrol.2010.07.012

Mohseni, F., Amani, M., Mohammadpour, P., Kakooei, M., Jin, S., & Moghimi, A. (2023). Wetland mapping in Great Lakes using Sentinel-1/2 time-series imagery and DEM data in Google Earth Engine. *Remote Sensing, 15*, 3495. https://doi.org/10.3390/rs15143495

Möller, R., & Hoffmann, H. (2004). An extension of neural gas to local PCA. *Neurocomputing, 62*, 305–326. https://doi.org/10.1016/j.neucom.2003.09.014

Mugabe, P. A., Mwaniki, F., Mamary, K. A., Ngibuini, H. M., (2019). An assessment of drought monitoring and early warning systems in Tanzania, Kenya, and Mali, in: Current Directions in Water Scarcity Research. Elsevier, pp. 211–219. https://doi.org/10.1016/B978-0-12-814820-4.00014-6

Mullissa, A., Vollrath, A., Odongo-Braun, C., Slagter, B., Balling, J., Gou, Y., Gorelick, N., & Reiche, J. (2021). Sentinel-1 SAR backscatter analysis ready data preparation in Google Earth Engine. *Remote Sensing, 13*, 1954. https://doi.org/10.3390/rs13101954

Mutsotso, R. B., Sichangi, A. W., & Makokha, G. O. (2018). Spatio-temporal drought characterization in Kenya from 1987 to 2016. *ARS, 07*, 125–143. https://doi.org/10.4236/ars.2018.72009

Najibi, N., & Jin, S. (2013). Physical reflectivity and polarization characteristics for snow and ice-covered surfaces interacting with GPS signals. *Remote Sensing, 5*, 4006–4030. https://doi.org/10.3390/rs5084006

Nasirzadehdizaji, R., Cakir, Z., Balik Sanli, F., Abdikan, S., Pepe, A., & Calò, F. (2021). Sentinel-1 interferometric coherence and backscattering analysis for crop monitoring. *Computers and Electronics in Agriculture, 185*, 106118. https://doi.org/10.1016/j.compag.2021.106118

Nguyen, H., Wheeler, M. C., Otkin, J. A., Nguyen-Huy, T., & Cowan, T. (2023). Climatology and composite evolution of flash drought over Australia and its vegetation impacts. *Journal of Hydrometeorology, 24*, 1087–1101. https://doi.org/10.1175/JHM-D-22-0033.1

De Ocampo, A.L.P., (2023). Normalized Difference Vegetation Index (NDVI) Estimation based on filter augmented imaging, in: 2023 International Electrical Engineering Congress (iEECON). Presented at the 2023 International Electrical Engineering Congress (iEECON), IEEE, pp. 84–88. https://doi.org/10.1109/iEECON56657.2023.10126616

Ochieng, P., Nyandega, I., & Wambua, B. (2022). Spatial-temporal analysis of historical and projected drought events over Isiolo County, Kenya. *Theoretical and Applied Climatology, 148*, 531–550. https://doi.org/10.1007/s00704-022-03953-5

Ochieng, P. O., Nyandega, I., Wambua, B., & Ongoma, V. (2023). Linkages between Madden–Julian oscillation and drought events over Kenya. *Meteorology and Atmospheric Physics, 135*, 9. https://doi.org/10.1007/s00703-022-00948-9

Olivieri, A. C., (2024). Introduction to multivariate calibration: A practical approach. Springer International Publishing, Cham. https://doi.org/10.1007/978-3-031-64144-2

Ondiko, J. H., & Karanja, A. M. (2021). Spatial and temporal occurrence and effects of droughts on crop yields in Kenya. *Oalib, 08*, 1–13. https://doi.org/10.4236/oalib.1107354

Opiyo, F. E., Wasonga, O. V., & Nyangito, M. M. (2014). Measuring household vulnerability to climate-induced stresses in pastoral rangelands of Kenya: Implications for resilience programming. *Pastoralism, 4*, 10. https://doi.org/10.1186/s13570-014-0010-9

Palagiri, H., & Pal, M. (2024). Parametric and non-parametric indices for agricultural drought assessment using ESACCI soil moisture data over the Southern Plateau and Hills, India. *International Journal of Applied Earth Observation and Geoinformation, 134*, 104175. https://doi.org/10.1016/j.jag.2024.104175

Palmer, & Wayne. (1965). *Meteorological Drought*. Weather Bureau, US Department of Commerce, Weather Bureau: US Department of Commerce.

Pande, C. B., Egbueri, J. C., Costache, R., Sidek, L. M., Wang, Q., Alshehri, F., Din, N. M., Gautam, V. K., & Chandra Pal, S. (2024). Predictive modeling of land surface temperature (LST) based on Landsat-8 satellite data and machine learning models for sustainable development. *Journal of Cleaner Production, 444*, 141035. https://doi.org/10.1016/j.jclepro.2024.141035

Pande, C. B., Moharir, K. N., Singh, S. K., Pham, Q. B., Elbeltagi, A. (Eds.), 2023. Climate change impacts on natural resources, ecosystems and agricultural systems, Springer Climate. Springer International Publishing, Cham. https://doi.org/10.1007/978-3-031-19059-9

Pei, F., Wu, C., Liu, X., Li, X., Yang, K., Zhou, Y., Wang, K., Xu, L., & Xia, G. (2018). Monitoring the vegetation

activity in China using vegetation health indices. *Agricultural and Forest Meteorology, 248*, 215–227. https://doi.org/10.1016/j.agrformet.2017.10.001

Phiri, D., Simwanda, M., Salekin, S., Nyirenda, V., Murayama, Y., & Ranagalage, M. (2020). Sentinel-2 data for land cover/use mapping: A review. *Remote Sensing, 12*, 2291. https://doi.org/10.3390/rs12142291

Price, J., Warren, R., Forstenhäusler, N., Wallace, C., Jenkins, R., Osborn, T. J., & Van Vuuren, D. P. (2022). Quantification of meteorological drought risks between 1.5 °C and 4 °C of global warming in six countries. *Climatic Change, 174*, 12. https://doi.org/10.1007/s10584-022-03359-2

Qin, Q., Wu, Z., Zhang, T., Sagan, V., Zhang, Z., Zhang, Y., Zhang, C., Ren, H., Sun, Y., Xu, W., & Zhao, C. (2021). Optical and thermal remote sensing for monitoring agricultural drought. *Remote Sensing, 13*, 5092. https://doi.org/10.3390/rs13245092

Quiring, S. M., & Ganesh, S. (2010). Evaluating the utility of the Vegetation Condition Index (VCI) for monitoring meteorological drought in Texas. *Agricultural and Forest Meteorology, 150*, 330–339. https://doi.org/10.1016/j.agrformet.2009.11.015

Ren, J., Shao, Y., Wan, H., Xie, Y., & Campos, A. (2021). A two-step mapping of irrigated corn with multi-temporal MODIS and Landsat analysis ready data. *ISPRS Journal of Photogrammetry and Remote Sensing, 176*, 69–82. https://doi.org/10.1016/j.isprsjprs.2021.04.007

Rhyma, P. P., Norizah, K., Hamdan, O., Faridah-Hanum, I., & Zulfa, A. W. (2020). Integration of Normalised Different Vegetation Index and Soil-Adjusted Vegetation Index for mangrove vegetation delineation. *Remote Sensing Applications: Society and Environment, 17*, 100280. https://doi.org/10.1016/j.rsase.2019.100280

Sakellariou, S., Spiliotopoulos, M., Alpanakis, N., Faraslis, I., Sidiropoulos, P., Tziatzios, G. A., Karoutsos, G., Dalezios, N. R., & Dercas, N. (2024). Spatiotemporal drought assessment based on gridded standardized precipitation index (SPI) in Vulnerable Agroecosystems. *Sustainability, 16*, 1240. https://doi.org/10.3390/su16031240

Sánchez, N., González-Zamora, Á., Piles, M., & Martínez-Fernández, J. (2016). A New Soil Moisture Agricultural Drought Index (SMADI) integrating MODIS and SMOS products: A case of study over the Iberian Peninsula. *Remote Sensing, 8*, 287. https://doi.org/10.3390/rs8040287

Sardooi, E. R., Azareh, A., Damaneh, H. E., & Damaneh, H. E. (2021). Drought monitoring using MODIS land surface temperature and normalized difference vegetation index products in semi-arid areas of Iran. *Journal of Rangeland Science, 11*, 402–418.

Schwabe, K., Albiac, J., Connor, J. D., Hassan, R. M., Meza González, L. (Eds.), (2013). Drought in arid and semi-arid regions: A multi-disciplinary and cross-country perspective. Springer Netherlands, Dordrecht. https://doi.org/10.1007/978-94-007-6636-5

Schwartz, C., Ellenburg, W. L., Mishra, V., Mayer, T., Griffin, R., Qamer, F., Matin, M., & Tadesse, T. (2022). A statistical evaluation of Earth-observation-based composite drought indices for a localized assessment of agricultural drought in Pakistan. *International Journal of Applied Earth Observation and Geoinformation, 106*, 102646. https://doi.org/10.1016/j.jag.2021.102646

Shahzaman, M., Zhu, W., Bilal, M., Habtemicheal, B. A., Mustafa, F., Arshad, M., Ullah, I., Ishfaq, S., & Iqbal, R. (2021). Remote sensing indices for spatial monitoring of agricultural drought in South Asian countries. *Remote Sensing, 13*, 2059. https://doi.org/10.3390/rs13112059

Shen, Z., Zhang, Q., Singh, V. P., Sun, P., Song, C., & Yu, H. (2019). Agricultural drought monitoring across Inner Mongolia, China: Model development, spatiotemporal patterns and impacts. *Journal of Hydrology, 571*, 793–804. https://doi.org/10.1016/j.jhydrol.2019.02.028

Shorachi, M., Kumar, V., & Steele-Dunne, S. C. (2022). Sentinel-1 SAR backscatter response to agricultural drought in The Netherlands. *Remote Sensing, 14*, 2435. https://doi.org/10.3390/rs14102435

Shrestha, B., OHara, C., Mali, P., (2009). Multi-sensor & Temporal data fusion for cloud-free vegetation index composites, in: Milisavljevic, N. (Ed.), Sensor and Data Fusion. I-Tech Education and Publishing. https://doi.org/10.5772/6582

Skakun, S., Kussul, N., Shelestov, A., & Kussul, O. (2016). The use of satellite data for agriculture drought risk quantification in Ukraine. *Geomatics, Natural Hazards and Risk, 7*, 901–917. https://doi.org/10.1080/19475705.2015.1016555

Small, D. (2011). Flattening gamma: Radiometric terrain correction for SAR imagery. *IEEE Trans. Geosci. Remote Sensing, 49*, 3081–3093. https://doi.org/10.1109/TGRS.2011.2120616

Son, B., Park, S., Im, J., Park, S., Ke, Y., & Quackenbush, L. J. (2021). A new drought monitoring approach: Vector projection analysis (VPA). *Remote Sensing of Environment, 252*, 112145. https://doi.org/10.1016/j.rse.2020.112145

Song, B., & Park, K. (2020). Detection of aquatic plants using multispectral UAV imagery and vegetation index. *Remote Sensing, 12*, 387. https://doi.org/10.3390/rs12030387

Sriwongsitanon, N., Gao, H., Savenije, H. H. G., Maekan, E., Saengsawang, S., & Thianpopirug, S. (2016). Comparing the Normalized Difference Infrared Index (NDII) with root zone storage in a lumped conceptual model. *Hydrology and Earth System Sciences, 20*, 3361–3377. https://doi.org/10.5194/hess-20-3361-2016

Sudmanns, M., Tiede, D., Augustin, H., & Lang, S. (2020). Assessing global Sentinel-2 coverage dynamics and data availability for operational Earth observation (EO) applications using the EO-Compass. *International Journal of Digital Earth, 13*, 768–784. https://doi.org/10.1080/17538947.2019.1572799

Taddeo, S., Dronova, I., & Depsky, N. (2019). Spectral vegetation indices of wetland greenness: Responses to vegetation structure, composition, and spatial distribution. *Remote Sensing of Environment, 234*, 111467. https://doi.org/10.1016/j.rse.2019.111467

Tadesse, T., Champagne, C., Wardlow, B. D., Hadwen, T. A., Brown, J. F., Demisse, G. B., Bayissa, Y. A., & Davidson, A. M. (2017). Building the vegetation drought response index for Canada (VegDRI-Canada) to monitor agricultural

drought: First results. *Giscience & Remote Sensing, 54*, 230–257. https://doi.org/10.1080/15481603.2017.1286728

Tanarhte, M., De Vries, A. J., Zittis, G., & Chfadi, T. (2024). Severe droughts in North Africa: A review of drivers, impacts and management. *Earth-Science Reviews, 250*, 104701. https://doi.org/10.1016/j.earscirev.2024.104701

Tang, H., Li, Z.-L., (2014). Quantitative remote sensing in thermal infrared: Theory and applications, Springer Remote Sensing/Photogrammetry. Springer Berlin Heidelberg, Berlin, Heidelberg. https://doi.org/10.1007/978-3-642-42027-6

Tao, H., Yaseen, Z. M., Tan, M. L., Goliatt, L., Heddam, S., Halder, B., Sa'adi, Z., Ahmadianfar, I., Homod, R. Z., & Shahid, S. (2024). High-resolution remote sensing data-based urban heat island study in Chongqing and Changde City, China. *Theoretical and Applied Climatology, 155*, 7049–7076. https://doi.org/10.1007/s00704-024-05041-2

Teluguntla, P., Thenkabail, P. S., Oliphant, A., Xiong, J., Gumma, M. K., Congalton, R. G., Yadav, K., & Huete, A. (2018). A 30-m landsat-derived cropland extent product of Australia and China using random forest machine learning algorithm on Google Earth Engine cloud computing platform. *ISPRS Journal of Photogrammetry and Remote Sensing, 144*, 325–340. https://doi.org/10.1016/j.isprsjprs.2018.07.017

Thenkabail, P. S., Ward, A. D., & Lyon, J. G. (1994). Landsat-5 Thematic Mapper models of soybean and corn crop characteristics. *International Journal of Remote Sensing, 15*, 49–61. https://doi.org/10.1080/01431169408954050

Tian, L., Yuan, S., & Quiring, S. M. (2018). Evaluation of six indices for monitoring agricultural drought in the south-central United States. *Agricultural and Forest Meteorology, 249*, 107–119. https://doi.org/10.1016/j.agrformet.2017.11.024

Tran, H. T., Campbell, J. B., Tran, T. D., & Tran, H. T. (2017). Monitoring drought vulnerability using multi-spectral indices observed from sequential remote sensing (Case Study: Tuy Phong, Binh Thuan, Vietnam). *Giscience & Remote Sensing, 54*, 167–184. https://doi.org/10.1080/15481603.2017.1287838

Trnka, M., Hlavinka, P., Možný, M., Semerádová, D., Štěpánek, P., Balek, J., Bartošová, L., Zahradníček, P., Bláhová, M., Skalák, P., Farda, A., Hayes, M., Svoboda, M., Wagner, W., Eitzinger, J., Fischer, M., & Žalud, Z. (2020). Czech Drought Monitor System for monitoring and forecasting agricultural drought and drought impacts. *International Journal of Climatology, 40*, 5941–5958. https://doi.org/10.1002/joc.6557

Uhe, P., Philip, S., Kew, S., Shah, K., Kimutai, J., Mwangi, E., Van Oldenborgh, G.J., Singh, R., Arrighi, J., Jjemba, E., Cullen, H., Otto, F., (2018). Attributing drivers of the 2016 Kenyan drought. International Journal of Climatology 38. https://doi.org/10.1002/joc.5389

Urban, M., Berger, C., Mudau, T. E., Heckel, K., Truckenbrodt, J., Onyango Odipo, V., Smit, I. P. J., & Schmullius, C. (2018). Surface moisture and vegetation cover analysis for drought monitoring in the Southern Kruger National Park using Sentinel-1, Sentinel-2, and Landsat-8. *Remote Sensing, 10*, 1482. https://doi.org/10.3390/rs10091482

Vicente-Serrano, S. M., Beguería, S., & López-Moreno, J. I. (2010). A multiscalar drought index sensitive to global warming: The standardized precipitation evapotranspiration index. *Journal of Climate, 23*, 1696–1718. https://doi.org/10.1175/2009JCLI2909.1

Vijayasekaran, D. (2019). SEN2-AGRI – crop type mapping pilot study using Sentinel-2 satellite imagery in India. *The International Archives of the Photogrammetry Remote Sensing and Spatial Information Sciences, XLII-3/W6*, 175–180. https://doi.org/10.5194/isprs-archives-XLII-3-W6-175-2019

Vreugdenhil, M., Wagner, W., Bauer-Marschallinger, B., Pfeil, I., Teubner, I., Rüdiger, C., & Strauss, P. (2018). Sensitivity of Sentinel-1 backscatter to vegetation dynamics: An Austrian case study. *Remote Sensing, 10*, 1396. https://doi.org/10.3390/rs10091396

West, H., Quinn, N., & Horswell, M. (2019). Remote sensing for drought monitoring & impact assessment: Progress, past challenges and future opportunities. *Remote Sensing of Environment, 232*, 111291. https://doi.org/10.1016/j.rse.2019.111291

Winkler, K., Gessner, U., & Hochschild, V. (2017). Identifying droughts affecting agriculture in Africa based on remote sensing time series between 2000–2016: Rainfall anomalies and vegetation condition in the context of ENSO. *Remote Sensing, 9*, 831. https://doi.org/10.3390/rs9080831

Wu, D., Qu, J. J., & Hao, X. (2015). Agricultural drought monitoring using MODIS-based drought indices over the USA Corn Belt. *International Journal of Remote Sensing, 36*, 5403–5425. https://doi.org/10.1080/01431161.2015.1093190

Wu, D., Li, Z., Zhu, Y., Li, X., Wu, Y., & Fang, S. (2021). A new agricultural drought index for monitoring the water stress of winter wheat. *Agricultural Water Management, 244*, 106599. https://doi.org/10.1016/j.agwat.2020.106599

Xue, J., & Su, B. (2017). Significant remote sensing vegetation indices: A review of developments and applications. *Journal of Sensors, 2017*, 1–17. https://doi.org/10.1155/2017/1353691

Younes, M. A., & Bakry, A. (2022). The 4.2 ka BP climate event in Egypt: Integration of archaeological, geoarchaeological, and bioarchaeological evidence. *African Archaeological Review, 39*, 315–344. https://doi.org/10.1007/s10437-022-09487-5

Zeng, L., Wardlow, B. D., Hu, S., Zhang, X., Zhou, G., Peng, G., Xiang, D., Wang, R., Meng, R., & Wu, W. (2021). A novel strategy to reconstruct NDVI time-series with high temporal resolution from MODIS multi-temporal composite products. *Remote Sensing, 13*, 1397. https://doi.org/10.3390/rs13071397

Zhang, A., & Jia, G. (2013). Monitoring meteorological drought in semiarid regions using multi-sensor microwave remote sensing data. *Remote Sensing of Environment, 134*, 12–23. https://doi.org/10.1016/j.rse.2013.02.023

Zhang, L., & Zhou, T. (2015). Drought over East Asia: A review. *Journal of Climate, 28*, 3375–3399. https://doi.org/10.1175/JCLI-D-14-00259.1

Zhang, N., Hong, Y., Qin, Q., & Liu, L. (2013). VSDI: A visible and shortwave infrared drought index for monitoring soil and vegetation moisture based on optical remote sensing. *International Journal of Remote Sensing, 34*, 4585–4609. https://doi.org/10.1080/01431161.2013.779046

Zhang, L., Jiao, W., Zhang, H., Huang, C., & Tong, Q. (2017a). Studying drought phenomena in the Continental United States in 2011 and 2012 using various drought indices. *Remote Sensing of Environment, 190*, 96–106. https://doi.org/10.1016/j.rse.2016.12.010

Zhang, X., Chen, N., Li, J., Chen, Z., & Niyogi, D. (2017b). Multi-sensor integrated framework and index for agricultural drought monitoring. *Remote Sensing of Environment, 188*, 141–163. https://doi.org/10.1016/j.rse.2016.10.045

Zhang, Z., Xu, W., Shi, Z., & Qin, Q. (2021). Establishment of a comprehensive drought monitoring index based on multisource remote sensing data and agricultural drought monitoring. IEEE J. *Sel. Top. Appl. Earth Observations Remote Sensing, 14*, 2113–2126. https://doi.org/10.1109/JSTARS.2021.3052194

Zhao, X., Sheisha, H., Thomas, I., Salem, A., Sun, Q., Liu, Y., Mashaly, H., Nian, X., Chen, J., Finlayson, B., & Chen, Z. (2021). Climate-driven early agricultural origins and development in the Nile Delta. *Egypt. Journal of Archaeological Science, 136*, 105498. https://doi.org/10.1016/j.jas.2021.105498

Zhou, L., Wu, J., Zhang, J., Leng, S., Liu, M., Zhang, J., Zhao, L., Zhang, F., & Shi, Y. (2013). The integrated surface drought index (ISDI) as an indicator for agricultural drought monitoring: Theory, validation, and application in Mid-Eastern China. *IEEE Journal of Selected Topics in Applied Earth Observations Remote Sensing, 6*, 1254–1262. https://doi.org/10.1109/JSTARS.2013.2248077